

45 Abstract

46 Endothelial cell (EC) barrier disruption induced by inflammatory agonists such as
47 thrombin leads to potentially lethal physiological dysfunction such as alveolar flooding,
48 hypoxemia and pulmonary edema. Thrombin stimulates paracellular gap and F-actin stress fiber
49 formation, triggers actomyosin contraction and alters EC permeability through multiple
50 mechanisms that include protein kinase C (PKC) activation. We previously have shown that the
51 ezrin, radixin, and moesin (ERM) actin-binding proteins differentially participate in S1P-induced
52 EC barrier enhancement. Phosphorylation of a conserved threonine residue in the C terminus of
53 ERM proteins causes conformational changes in ERM to unmask binding sites and is considered
54 a hallmark of ERM activation. In the present study we test the hypothesis that ERM proteins are
55 phosphorylated on this critical threonine residue by thrombin-induced signaling events and
56 explore the role of the ERM family in modulating thrombin-induced cytoskeletal rearrangement
57 and EC barrier function. Thrombin promotes ERM phosphorylation at this threonine residue
58 (Ezrin-567, Radixin-564, Moesin-558) in a PKC-dependent fashion and induces translocation of
59 phosphorylated ERM to the EC periphery. Thrombin-induced ERM threonine phosphorylation is
60 likely synergistically mediated by protease-activated receptors PAR₁ and PAR₂. Using the
61 siRNA approach, depletion of either moesin alone, or of all three ERM proteins, significantly
62 attenuates thrombin-induced increase in EC barrier permeability (TER), cytoskeletal
63 rearrangements, paracellular gap formation and accumulation of di-phospho-MLC. In contrast,
64 radixin depletion exerts opposing effects on these indices. These data suggest that ERM proteins
65 play important differential roles in the thrombin-induced modulation of EC permeability, with
66 moesin promoting barrier dysfunction and radixin opposing it.

67 **Keywords:** thrombin; ERM; PKC; phosphorylation; endothelial cells; barrier dysfunction;
68 cytoskeleton

69

70

71

72

73

74

75

76

77

78

79

80

81

82

83

84

85

86

87

88

89

90 **Abbreviations:** ERM, ezrin, radixin, and moesin proteins; PKC, protein kinase C; Thr, thrombin

91

92 **Introduction**

93 The pulmonary vascular endothelium serves as a semi-selective barrier between circulating
94 blood and surrounding tissues. Endothelial cell (EC) barrier integrity is therefore critical to tissue
95 and organ function. Disruption of the endothelial barrier by inflammatory mediators such as
96 thrombin, histamine, and LPS leads to potentially lethal physiological dysfunction such as
97 hypoxemia, atherosclerosis and pulmonary edema, a hallmark of acute lung injury and its more
98 severe form, acute respiratory distress syndrome (12). Therefore, the preservation of vascular
99 endothelial cell (EC) barrier integrity has the potential for profound clinical impact. Multiple
100 studies have demonstrated that inflammation-induced EC barrier dysfunction involves
101 cytoskeletal rearrangement, contraction of endothelial cells and intercellular gap formation,
102 leading to increased paracellular permeability (18, 20, 55, 65). Thrombin, a multifunctional
103 serine protease, proteolytically cleaves and activates PAR₁, a member of a unique class of G
104 protein-coupled receptors activated by proteolytic cleavage of their extracellular N-terminal
105 domains and expressed at the surfaces of EC (43, 66). Thrombin can transactivate PAR₂ through
106 PAR₁ in cultured human umbilical vein EC (HUVECs) (48). PAR₁ and PAR₂ activate
107 heterotrimeric G-proteins G_q, G_{12/13}, and G_i, all of which are involved in permeability regulation
108 (42). Activation of G_q mobilizes Ca²⁺ and activates PKC, RhoA, and EC contraction, resulting in
109 endothelial barrier disruption.

110 The widely distributed ERM family of membrane-associated proteins (ezrin, radixin,
111 moesin) regulates the structure and function of specific domains of the cell cortex [reviewed in
112 (2, 14, 46)]. The ERM proteins are actin-binding linkers that connect the actin cytoskeleton to
113 the plasma membrane. This linker function makes ERM proteins essential for many fundamental
114 cellular processes including cell adhesion, determination of cell shape, motility, cytokinesis and
115 integration of membrane transport with signaling pathways (14, 47, 71). The three ERM proteins

116 share a high level of amino acid identity (70-85%) (14), and prior to activation exist in an auto-
117 inhibited conformation in which the actin-binding C-terminal tail binds and masks the N-
118 terminal FERM domain (band 4.1, ezrin, radixin, moesin homology domains) (50). The
119 activation state of ERM proteins is tightly regulated by phosphorylation events. Binding of the
120 protein to membrane lipid phosphatidylinositol 4,5-bisphosphate (PIP₂) (15) and subsequent
121 phosphorylation of a conserved C-terminal threonine (T567 in ezrin, T564 in radixin, T558 in
122 moesin) (21, 41, 50) are believed to disrupt the intramolecular association, thus unmasking sites
123 for interactions with other proteins. In addition, phosphorylation of ezrin on other residues may
124 be required to direct specific targeted effects in cells (29, 36, 57). Several kinases have been
125 implicated in regulating ERM protein function through phosphorylation of the C-terminal
126 threonine residue (3, 10, 35, 40, 59, 67). However, the identity of kinases that directly
127 phosphorylate ERM in many cells remains to be clearly defined (14, 29).

128 ERM proteins also associate with cytoplasmic signaling molecules in cellular processes
129 that require membrane cytoskeletal reorganization. ERM proteins appear to act both downstream
130 and upstream of the Rho family of GTPases, which regulates remodeling of the actin
131 cytoskeleton (14, 29). However, information is limited concerning the possible role of ERM
132 proteins in the remodeling of endothelial cytoskeleton in response to different agonists. Koss and
133 coworkers (35) demonstrated that ERM proteins are phosphorylated on C-terminal threonine
134 residues by TNF- α -induced signaling events and likely play important roles in modulating the
135 cytoskeletal changes and permeability increases in human pulmonary microvascular EC. We
136 previously have shown that PKC isoforms are required for ERM phosphorylation in human
137 pulmonary EC induced by the potent barrier protective factor, platelet-derived phospholipid
138 sphingosine-1 phosphate (S1P) (1). Further, we previously demonstrated that ERM proteins,

139 despite their structural similarities and reported functional redundancy, differentially modulate
140 SIP-induced changes in lung EC cytoskeleton and permeability (1). In the present study, we
141 explored the potential involvement of ERM proteins in modulating thrombin-induced
142 cytoskeletal rearrangement and EC barrier function.

143

144 **Materials and methods**

145

146 **Reagents**

147 Thrombin was obtained from Sigma Co. (St. Louis, MO). Antibodies (Ab) were obtained as
148 follows: mouse monoclonal Ab against β -Tubulin (Covance, Berkeley, CA), rabbit polyclonal
149 di-phospho-MLC and rabbit polyclonal phospho-Ezrin (Thr567)/Radixin (Thr564)/Moesin
150 (Thr558) Ab (Cell Signaling, Danvers, MA), ezrin specific mouse monoclonal Ab (Invitrogen
151 Life Technologies, Carlsbad, CA), rabbit monoclonal anti-radixin Ab (Sigma, St. Louis, MO),
152 mouse monoclonal anti-moesin Ab (BD Biosciences, San Jose, CA), mouse monoclonal anti-
153 thrombin receptor WEDE15 blocking Ab (Beckman Coulter, Indianapolis, IN), mouse
154 monoclonal thrombin R (ATAP2) blocking Ab (Santa Cruz Biotech., Santa Cruz, CA), Texas red
155 phalloidin and Alexa 488-, Alexa 594-conjugated secondary Ab (Molecular Probes, Eugene,
156 OR). ROCK inhibitors Y-27632 and H-1152, PKC inhibitors Ro-31-7549, Bisindolylmaleimide
157 I, and Go 6976, p38 kinase inhibitor SB203580 were purchased from Calbiochem (San Diego,
158 CA), Ca^{2+} chelator BAPTA-AM was obtained from Sigma (St. Louis, MO), PI3 Kinase
159 inhibitor LY294002 and MLCK inhibitor ML-7, PAR_1 selective agonist TFLLR-NH₂, PAR_2
160 selective agonist SLIGRL-NH₂ and reversed amino acid sequence control peptides RLLFT-NH₂

161 and LRGILS-NH₂ were obtained from TOCRIS (Bristol, UK). Unless specified, biochemical
162 reagents were obtained from Sigma.

163

164 **Cell culture**

165 Human pulmonary artery endothelial cells (HPAEC) were obtained from Lonza Inc.
166 (Walkersville, MD) and were utilized at passages 5–9.

167

168 **Measurement of transendothelial electrical resistance**

169 Cellular barrier properties were measured using an electrical cell substrate impedance
170 sensing system (ECIS) (Applied Biophysics, Troy, NY). HPAEC were seeded onto plates with
171 small gold electrodes (10–4 cm²) and measurements of transendothelial electrical resistance
172 (TER) across confluent HPAEC monolayers were performed as previously described (6, 19, 65).

173

174 **Real-time quantitative RT–PCR**

175 Endogenous transcript levels of ezrin (*EZR*), radixin (*RDX*), and moesin (*MSN*) in HPAEC
176 were measured in a 384-well PCR plate with an ABI 7900 HT Fast Real-Time PCR System
177 (Applied Biosystems, Carlsbad, CA). Total RNA (1 µg) were first reverse transcribed using
178 Superscript II Reverse Transcriptase (Invitrogen Life Technologies) and random hexamer
179 primers (Applied Biosystems) to generate cDNA. Quantitative Real Time-PCR (qRT-PCR) was
180 then performed using the Assay-on-Demand system (Hs00185574_m1 (*EZR*); Hs00267954_m1
181 (*RDX*); Hs00792607_mH (*MSN*) from Applied Biosystems according to the manufacturer's
182 protocol. Purity and specificity of all products were confirmed by omitting the reverse
183 transcriptase or template. Analysis of results is based on the average of triplicates. The standard

184 curve method was used for relative quantitation of target gene expression. Further information on
 185 the method can be found on User Bulletin #2 on the ABI website.

186

187 **Depletion of specific EC proteins via siRNA**

188

189 To reduce the content of individual EC proteins, cultured EC were treated with specific
 190 siRNA duplexes, which guide sequence-specific degradation of the homologous mRNA (13).

191 The following validated siRNAs were obtained from QIAGEN (Valencia, CA) in ready-to-use,

192 desalted, and duplexed form: duplex of sense 5'-CACCGUGGGAUGCUCAAAGdTdT-3' and

193 antisense 5'-CUUUGAGCAUCCCACGGUGdTdT-3' siRNA was used for targeting sequences

194 that are part of the coding region for Homo sapiens ezrin: 5'-

195 AACACCGTGGGATGCTCAAAG-3', duplex of sense 5'-

196 GAAUAACCCAGAGACUCUdTdT-3' and antisense 5'-

197 AGAGUCUCUGGGUUAUUUCdTdT-3' was used for targeting sequences that are part of the

198 coding region for Homo sapiens radixin: 5'-AAGAAATAACCCAGAGACTCT-3', and duplex

199 of sense 5'-GGGAUGUCAACUGACCUAAdTdT-3' and antisense 5'-

200 UUAGGUCAGUUGACAUCCCdTdT-3' was used for targeting sequences that are part of the

201 coding region for Homo sapiens moesin: 5'-CAGGGATGTCAACTGACCTAA-3'. Duplex of

202 sense 5'-AGAGCUAAG-UAGAUGUGUAdTdT-3' and antisense 5'-

203 UACACAUCUACUUAGCUCUdTdT-3' siRNA was used for targeting sequences that are part

204 of the coding region for Homo sapiens PKC β I: 5'-CAAGAGCTAAGTAGATGTGTA-3', duplex

205 of sense 5'-GAAGCAUGACAGCAUAAA dTdT-3' and antisense 5'-

206 UUUAAUGCUGUCAUGCUUCdCdG-3' was used for targeting sequences that are part of the

207 coding region for Homo sapiens PKC ζ : 5'-CGGAAGCATGACAGCATTAAA-3', duplex of

208 sense 5'-CUCUACCGUGCCACGUUUUdTdT-3' and antisense 5'-
209 AAAACGUGGCACGGUAGAGdTdT-3' was used for targeting sequences that are part of the
210 coding region for Homo sapiens PKC δ : 5'-AACTCTACCGTGCCACGTTTT-3', duplex of sense
211 5'-CAAGAAGUGUAUUGAUAAAAdTdT-3' and antisense 5'-
212 UUUUAUCAAUACACUUCUUGdTdG-3' was used for targeting sequences that are part of the
213 coding region for Homo sapiens PKC θ : 5'-CACAAGAAGTGTATTGATAAAA-3', duplex of
214 sense 5'- CGGAAACACCCGUACCUUAdTdT-3' and antisense 5'-
215 UAAGGUACGGGUGUUUCCGdTdG-3' were used for targeting sequences that are part of the
216 coding region for Homo sapiens PKC ϵ : 5'- CACGGAAACACCCGTACCTTA-3'. Silencer
217 select pre-designed siRNA duplex (Life Technologies, Grand Island, NY) of sense 5'-
218 CCCGUAACCUAUUUCCUAUdTdT-3' and antisense 5'-
219 AUAGGAAUUAGGUUACGGGdCdC-3' was used for targeting sequences that are part of the
220 coding region for Homo sapiens PKC γ : 5'- GGCCCGTAACCTAATTCCTAT-3'. Non-specific,
221 non-targeting AllStars siRNA duplex (QIAGEN, Valencia, CA) was used as negative control
222 treatment. HPAEC were grown to 70% confluence, and the transfection of siRNA (final
223 concentration 50 nM) was performed using DharmaFECT1 transfection reagent (Dharmacon
224 Research, Lafayette, CO) according to manufacturer's protocol. Forty eight hours post-
225 transfection cells were harvested and used for experiments. Additional control experiments using
226 EC transfections with fluorescently labeled nonspecific RNA showed that this protocol allowed
227 us to achieve 90–100% transfection efficiency.

228

229 **Plasmid Constructs**

230 Moesin constructs (wild type and phosphorylation deficient mutant) were prepared as we
231 have previously described (9).

232

233 **Immunofluorescent staining**

234 EC were plated on glass coverslips, grown to 70% confluence, and transfected with siRNA
235 followed by stimulation with thrombin. Then cells were fixed in 3.7% formaldehyde solution in
236 PBS for 10 min at 4°C, washed three times with PBS, permeabilized with 0.2% Triton X-100 in
237 PBS-Tween (PBST) for 30 min at room temperature, and blocked with 2% BSA in PBST for 30
238 min. Incubation with antibody of interest was performed in blocking solution for 1 h at room
239 temperature followed by staining with either Alexa 488-, or Alexa 594-conjugated secondary Ab
240 (Molecular Probes). Actin filaments were stained with Texas Red-conjugated phalloidin
241 (Molecular Probes) for 1 h at room temperature. After immunostaining, the glass slides were
242 analyzed using a Nikon video-imaging system (Nikon Instech Co., Japan) consisting of a phase
243 contrast inverted microscope Nikon Eclipse TE2000 connected to Hamamatsu (Hamamatsu
244 Photonics K.K., Japan) digital camera and image processor. The images were recorded and
245 processed using Adobe Photoshop 6.0.

246

247 **Immunoblotting**

248 Protein extracts were separated by 4-15% gradient SDS-PAGE, transferred to nitrocellulose
249 or polyvinylidene difluoride membranes (30 V for 18 h or 100 V for 1.5 h), and reacted with Ab
250 that recognizes ezrin, moesin, radixin, or other Ab of interest as indicated for individual
251 experiments. The level of phosphorylated ERM was examined by using a single Ab that
252 recognizes any of the three ERM proteins only when they are phosphorylated on the threonine

253 residue: ezrin (T567)/radixin (T564)/moesin (T558) (Cell Signaling). Immunoreactive proteins
254 were detected with the enhanced chemiluminescent detection system (ECL) according to the
255 manufacturer's directions (Amersham, Little Chalfont, UK). Intensities of immunoreactive
256 protein bands were quantified using ImageQuant software (Molecular Dynamics, Sunnyvale,
257 CA).

258

259 **Statistical Analysis**

260 Results are expressed as means \pm SD of three to six independent experiments. We
261 performed statistical comparison among treatment groups by unpaired Student's t-test or by
262 randomized-design two-way analysis of variance followed by the Newman-Keuls post hoc test
263 for multiple-groups. Results with $P < 0.05$ were considered statistically significant.

264

265 **Results**

266 **Expression of ezrin, radixin and moesin in HPAEC**

267 The mRNA expression profiles of individual ERMs were analyzed for confluent human
268 pulmonary EC. RT-PCR analysis reveals differential expression with highest relative expression
269 of moesin and lowest expression of radixin (Fig.1).

270

271 **Thrombin induces threonine phosphorylation of ERM via a PKC-mediated pathway**

272 To elucidate the effect of thrombin on phosphorylation of ERM at its critical C-terminal
273 threonine, confluent human pulmonary EC were stimulated with thrombin (0.5 U/ml), and
274 threonine phosphorylation then was evaluated by Western blot analysis utilizing phospho-
275 specific ERM antibody (phospho-Ezrin Thr567/Radixin Thr564/Moesin Thr558). Thrombin

276 induced the sustained threonine phosphorylation of ERM, which reached maximum levels by 5
277 min and remained elevated for at least 120 min (Fig. 2).

278 Because several kinases, including members of PKC, ROCK, GRK2, p38, Mst4 and LOK,
279 have been reported to phosphorylate the regulatory C-terminal threonine residue of ERM
280 proteins in various systems (3, 10, 35, 40, 59, 67), experiments were performed to determine the
281 signaling mechanisms leading to ERM phosphorylation in pulmonary EC upon thrombin
282 treatment. The role of different kinases was examined by using specific pharmacological
283 inhibitors: PKC-specific inhibitor Ro-31-7549, p38 MAPK inhibitor SB203580, Rho-associated
284 protein kinase (ROCK) inhibitor Y-27632, phosphoinositide 3-kinases (PI3Ks) inhibitor
285 LY294002, and chelator of intracellular Ca^{2+} BAPTA (Fig. 3). In our experiments, pretreatment
286 with Ro-31-7549 effectively prevented the increase in ERM phosphorylation induced by
287 thrombin (Fig. 3A), suggesting that this increase is PKC-dependent. Pretreatment with BAPTA,
288 a chelator of intracellular Ca^{2+} , partially inhibited ERM phosphorylation (Fig. 3A). We next
289 explored whether additional signaling pathways previously reported to participate in ERM
290 regulation are involved in thrombin-induced ERM phosphorylation. Pretreatment with Y-27632
291 did not exert a significant effect on ERM threonine phosphorylation. At the same time,
292 phosphorylation of myosin light chain (MLC), regulated by the ROCK/myosin phosphatase-
293 dependent signaling pathway, was significantly attenuated in ECs preincubated with Y-27632
294 (Fig. 3A). Because of the critical role of Rho activation, through its downstream effector ROCK,
295 in thrombin-induced EC barrier dysfunction, we next studied how the inhibition of ROCK affects
296 ERM phosphorylation using the more potent and selective cell-permeable pharmacological
297 ROCK inhibitor H-1152. Pretreatment with either H-1152 or Y-27632 did not exert significant
298 effects on ERM threonine phosphorylation after thrombin (Fig. 3B). In addition, preincubation of

299 HPAEC with the pharmacologic inhibitor of p38 MAPK SB203580 did not significantly affect
300 ERM phosphorylation (Fig. 3A, B).

301 The role of PKC isoforms was examined by using two alternative approaches: pretreatment
302 of EC with PKC-specific pharmacological inhibitors and using isoform-specific siRNAs. We
303 utilized three PKC-specific pharmacological inhibitors that have different IC_{50} values for
304 different PKC isoforms, bisindolylmaleimide I (BIM), Go 6976, and Ro-31-7549. Bis I, Ro-31-
305 7549 and Go 6970 are all competitive inhibitors for the ATP-binding site of PKC (39, 63, 69).
306 BIM inhibits the conventional PKC isoforms α , β I, β II and γ (activated by phosphatidylserine,
307 diacylglycerol and Ca^{2+}) with similar potency ($IC_{50} = 10$ nM) (63), and the unconventional
308 isoforms δ and ϵ (require phosphatidylserine and diacylglycerol but are Ca^{2+} -independent) and
309 the atypical isoform ζ (require only phosphatidylserine), to a lesser extent (39). In contrast to
310 BIM, Ro-31-7549 has slight selectivity for the α isoform ($IC_{50} = 53$ nM), but also affects β I, β II,
311 ϵ and γ (69). Go 6970 inhibits Ca^{2+} -dependent PKC isoforms α and β I (39). In our experiments,
312 pretreatment with Ro-31-7549, BIM and Go 6970 effectively suppressed ERM phosphorylation
313 induced by thrombin (Fig. 3C). These pharmacological PKC inhibitor data combined with the
314 BAPTA data suggest that multiple PKC isoforms may be required. Furthermore, our experiments
315 demonstrate that incubation with Go 6976 significantly inhibited phosphorylation of MLC at
316 Thr18 and Ser19 induced by thrombin (Fig. 3C).

317 To better characterize the PKC isoforms involved in ERM phosphorylation after
318 thrombin, activation of individual PKC kinases was explored using isoform-specific phospho-
319 antibodies. Thrombin stimulation (0.5 U/ml) of HPAEC significantly increased phosphorylation
320 of PKC β (Thr500) (Fig. 4A), PKC γ (Thr514) (Fig. 4B), PKC ϵ (Ser729) (Fig. 4C),
321 PKC ζ (Thr410) (Fig. 4D), PKC θ (Thr538) (Fig. 4E), and PKC δ (Tyr311) (Fig. 4F). Previous

322 studies have indicated that these PKC isoforms play important roles in thrombin- and other
323 inflammatory agonists- (TNF- α , IL-1 β , VEGF, hypoxia) induced modulation of endothelial
324 permeability (16, 38, 44, 51, 53, 56, 61, 62, 70) and therefore were selected for further
325 experimentation using isoform-specific siRNA. We first validated that these siRNAs efficiently
326 inhibit their respective targets: 65 \pm 7% depletion of PKC β , 97 \pm 2.2% depletion of PKC δ ,
327 75.5 \pm 2.4% depletion of PKC θ , 92 \pm 2.5% depletion of PKC ϵ , and 65 \pm 2.5% depletion of PKC γ
328 [Fig. 5, see also (1)]. It is important to note the limitations of this siRNA approach as it does not
329 provide 100% protein suppression and therefore some, albeit reduced protein function likely
330 remains. EC were transfected with siRNA for PKC β I, PKC γ , PKC ϵ , PKC ζ , PKC θ or PKC δ and
331 then stimulated with thrombin to determine the effects on ERM threonine phosphorylation.
332 Depletion of individual PKC γ , PKC ϵ , PKC ζ , PKC θ or PKC δ isoforms significantly reduced
333 ERM phosphorylation after thrombin (Fig. 6 A, B). To further clarify the involvement of PKC
334 activity in thrombin-induced ERM and MLC phosphorylation, we pursued simultaneous
335 depletion of several PKC isoforms (pan-PKC) via siRNA. Combined depletion of several PKC
336 isoforms markedly reduced ERM phosphorylation after thrombin (Fig. 6C, D), suggesting
337 possible cooperative regulation in this phosphorylation response. Moreover, downregulation of
338 pan-PKC significantly attenuates thrombin-induced MLC di-phosphorylation (Fig. 6C, E),
339 suggesting that multiple PKC isoforms may be involved. Taken together, these data indicate that
340 multiple PKC isoforms (conventional, unconventional and atypical) likely participate in
341 thrombin-induced ERM and MLC phosphorylation. One limitation of these data is that combined
342 silencing of multiple PKC isoforms may result in some nonspecific effects, e.g. nonspecific
343 activation or/and inhibition of other signaling pathways. Therefore, further studies utilizing

344 alternative approaches (e.g. isoform specific PKC peptide inhibitors) will be needed to verify
345 these findings.

346

347 **Effects of ERM depletion on thrombin-induced ERM threonine and MLC phosphorylation**

348 Numerous studies have reported a critical role for activation of the contractile apparatus in
349 specific models of agonist-induced EC barrier dysfunction [reviewed in (12)]. A key contractile
350 event in thrombin-induced barrier dysfunction is the phosphorylation of regulatory MLC,
351 catalyzed by Ca^2 /CaM-dependent MLCK (60, 72) and regulated by small GTPase Rho. There are
352 no antibodies currently available that specifically differentiate among the C-terminal phospho-
353 threonines of individual ERM proteins. Therefore, to assess the contribution of individual
354 proteins in total ERM threonine phosphorylation and their roles in MLC phosphorylation after
355 thrombin, we used siRNAs targeting ezrin, radixin, and moesin. We first validated that these
356 siRNAs efficiently and specifically inhibited their respective targets (1). Pulmonary EC were
357 then transfected with nonspecific siRNA, or siRNA for moesin, radixin, or siRNA for the
358 combination of ezrin, radixin and moesin (pan-ERM), and then stimulated with thrombin. Pan-
359 ERM and MLC phosphorylation was evaluated by Western blot analysis utilizing phospho-
360 specific ERM antibody and phospho-myosin light chain 2 (Thr18/Ser19) antibody (di-phospho-
361 MLC). In contrast to cells transfected with nonspecific RNA, depletion of moesin alone or
362 downregulation of pan-ERM significantly reduced time-dependent ERM and MLC
363 phosphorylation after thrombin (Fig. 7A, D). Thrombin-induced ERM and MLC phosphorylation
364 was partially attenuated by depletion of ezrin (Fig. 7C). In contrast, depletion of radixin did not
365 have any significant effect on MLC phosphorylation after thrombin (Fig. 7B). Radixin siRNA
366 partially, but significantly, reduced ERM threonine phosphorylation (Fig. 7B). Taken together,

367 these data indicate that in pulmonary EC thrombin induces primarily threonine phosphorylation
368 of moesin, followed by ezrin, and then radixin. These data also suggest that activated moesin and
369 to a lesser degree ezrin, but not radixin, may play a role in MLC phosphorylation induced by
370 thrombin via the ROCK/myosin phosphatase signaling pathway.

371

372 **Role of ERM in thrombin-induced lung EC hyperpermeability**

373 To evaluate the functional involvement of individual ERM proteins in thrombin-induced
374 EC barrier dysfunction, we measured changes in TER, a highly sensitive *in vitro* assay of
375 permeability, in lung EC treated with nonspecific siRNA or those treated with siRNA for ezrin,
376 radixin, or moesin (either singly or in combination). Comparing the data expressed as normalized
377 resistance (Fig. 8) to the time course of ERM threonine phosphorylation (Fig. 2) demonstrates
378 that the increase in ERM phosphorylation is highly correlated with the onset of thrombin-
379 induced hyperpermeability. Depletion of individual ERM proteins does not affect basal
380 permeability. However, the thrombin-induced decrease in TER is markedly attenuated in EC
381 transfected with moesin or pan-ERM-specific siRNA (Fig. 8A, D and E) compared with cells
382 transfected with nonspecific RNA duplexes. The initial thrombin-induced decrease in TER was
383 attenuated by siRNA depletion of ezrin, but this intervention markedly enhanced the recovery
384 above baseline in the later stage (Fig. 8C, E). In contrast, depletion of radixin slightly augments
385 the decrease in TER during the early phase and attenuates the later recovery phase after thrombin
386 (Fig. 8B, E) compared with agonist-stimulated cells transfected with nonspecific RNA. These
387 data clearly indicate differential roles for individual ERM proteins in mediating thrombin-
388 induced lung EC hyperpermeability.

389

390 **Role of PARs in thrombin-induced ERM phosphorylation**

391 In human pulmonary EC, activation of PAR₁ and PAR₂ promotes PKC and RhoA
392 activation and triggers the endothelial barrier-disruptive response (7, 22, 37, 43). We next
393 utilized PAR₁-specific blocking antibodies ATAP2 and WEDE15, and PAR₁ (TFLLR-NH₂) and
394 PAR₂ (SLIGRL-NH₂) selective agonist peptides, to determine the roles of these receptors in
395 thrombin-induced threonine phosphorylation of ERM. HPAEC preincubation with both ATAP2
396 and WEDE15, either singly or in combination, significantly decreased ERM phosphorylation
397 after thrombin relative to controls (Fig. 9). Stimulation of EC with both TFLLR-NH₂ and
398 SLIGRL-NH₂ augmented the phospho-ERM signal (Fig. 10) compared with cells treated with
399 control peptides. Interestingly, incubation of EC with a combination of TFLLR-NH₂ and
400 SLIGRL-NH₂ markedly enhanced ERM phosphorylation, compared with cells treated with these
401 two agonists alone (Fig. 10), suggesting that both PAR₁ and PAR₂ may have additive or
402 synergistic effects in this phosphorylation response.

403

404 **Involvement of ERM in thrombin-induced EC cytoskeletal remodeling**

405 Compromised barrier function induced by thrombin is tightly associated with actin
406 cytoskeletal rearrangements, F-actin stress fiber formation, increased MLCK-catalyzed MLC
407 phosphorylation spatially co-localized with stress fibers, actomyosin contraction, opening of
408 paracellular gaps, and hyperpermeability (12, 43). Within this context, the distribution of
409 phosphorylated ERM in EC before and after thrombin treatment was examined via
410 immunofluorescence. Before thrombin treatment, minimal phosphorylated ERM was observed in
411 the cytoplasm of pulmonary EC. In some areas of quiescent monolayers, phospho-ERM
412 localized in the spike-like structures overlapping the cell-cell contact areas (Fig. 11, image a,

413 arrow 1). Stimulation with thrombin induced an increase in the amount of phosphorylated ERM,
414 consistent with immunoblotting studies (Fig. 2). During the early response (5 minutes after initial
415 stimulation), phosphorylated ERM was localized primarily at the cell periphery and spike-like
416 areas (Fig. 11, image b, arrows 1 and 2) with a smaller amount of phospho-ERM also observed
417 in the cytoplasm (Fig. 11, image b). In contracting EC (15 minutes after initial challenge) the
418 phospho-ERM signal markedly increased in the peripheral cytoplasmic areas (Fig. 11, image c).
419 During partial restoration phases (60 and 120 minutes after the initial challenge), phosphorylated
420 ERM primarily localized in cytoplasmic areas and spike-like structures that were originally seen
421 in quiescent cells (Fig. 11, images d, e), but the overall level of phosphorylated ERM appeared
422 slightly elevated compared to baseline. These dynamic changes in phosphorylated ERM
423 localization during the phases of active cell contraction and partial barrier restoration indicate
424 that ERM proteins may play a role in both processes. The observation that phosphorylated ERM
425 proteins were primary concentrated along the EC periphery upon thrombin treatment led us to
426 examine the role of these proteins in modulating endothelial cytoskeletal rearrangements that
427 occur during thrombin-induced EC hyperpermeability.

428 In the next series of experiments we analyzed the effect of ERM depletion on the human
429 endothelial actin cytoskeleton. EC were transfected with nonspecific RNA duplex
430 oligonucleotides (Fig. 12) or ERM-specific siRNA (Fig. 12) followed by thrombin challenge (15
431 min, 0.5 U/ml). Double immunofluorescent staining using Texas red phalloidin to visualize F-
432 actin and di-phospho-MLC antibody to detect phosphorylated MLC was performed.
433 Unstimulated EC transfected with ezrin-, radixin-, or moesin-specific siRNAs, either individually
434 or in combination, demonstrated no significant differences in the organization of actin
435 cytoskeleton and levels of MLC phosphorylation compared with control EC exposed to

436 nonspecific RNA (Fig. 12, panel A, images a-n). However, thrombin stimulation of EC treated
437 with nonspecific RNA induced robust F-actin stress fiber and gap formation and accumulation of
438 di-phospho-MLC (Fig. 12, panel B, images c and d), which were nearly abolished by the
439 combination of siRNAs for radixin/ezrin/radixin (pan-ERM depletion), or by siRNA for moesin
440 alone. In contrast, radixin depletion alone slightly *enhanced* stress fiber formation and MLC
441 phosphorylation (Fig.12, panel B, images k and l). We next explored the effects of
442 overexpression of a phosphorylation-deficient mutant of moesin (Thr558Ala) on EC cytoskeletal
443 organization. Scanning densitometry (Fig. 13A) demonstrated relatively equivalent expression of
444 the wild type and mutant moesin in EC. Monolayers overexpressing mutant moesin exhibited
445 decreased F-actin stress fibers after thrombin and prominent cortical actin compared to EC
446 overexpressing wild type moesin (Fig.13, panel B, images c, g). These data together demonstrate
447 that ERM proteins are downstream targets of thrombin-induced signaling mechanisms and play
448 an essential and differential role in the regulation of the endothelial actomyosin cytoskeleton.

449

450 **Discussion**

451 Prior work has revealed that the procoagulant serine protease thrombin induces endothelial
452 barrier compromise through G protein-coupled Ca^{2+} mobilization, MLCK, PKC and RhoA
453 activation, which produces cytoskeletal rearrangement, dissociation of endothelial cell-cell
454 junctions as well as cytoskeleton contraction resulting in paracellular hyperpermeability (12, 27,
455 33, 34, 43, 45, 66). Although ERM proteins act as signal transducers for agonists that induce
456 cytoskeletal remodeling (14), the role of ERM in barrier regulation by thrombin is unknown.
457 Moesin is the most expressed ERM protein in several types of endothelial cells (4, 24, 30, 35).
458 Here we demonstrate that moesin is the most abundant ERM expressed in HPAEC as measured
459 by mRNA content, with radixin being the least expressed. We previously have shown that the

460 angiogenic sphingolipid S1P induces ERM phosphorylation on a conserved threonine residue
461 critical for ERM activation via a pathway that requires PKC, Rac1, Rho A, and p38 MAPK (1).
462 We also have previously demonstrated that phosphorylation of ERM in response to the
463 microtubule disruptor 2-methoxyestradiol (2ME) occurs in a p38/PKC-dependent manner
464 (9). We therefore explored whether the ERM family of proteins plays a role in modulating the
465 thrombin-induced endothelial barrier response. Our data demonstrate that thrombin increases
466 ERM phosphorylation at a critical regulatory threonine site in HPAEC monolayers and strongly
467 suggest important roles for the ERM proteins in mediating endothelial barrier dysfunction by
468 thrombin. This phosphorylation requires thrombin-induced signaling pathways that include
469 activation of PKC isoforms, but it is not regulated in a RhoA/ROCK- or p38-dependent manner.
470 Our results differ from those in our (1, 9), and others previous studies (23, 35, 68), in which the
471 phosphorylation of ERM was PKC-, RhoA/ROCK- and-p38-dependent in response to S1P,
472 PKC- and RhoA/ROCK-dependent in response to 2ME and TNF- α , and RhoA/ROCK-
473 dependent in response to advanced glycation end products (AGE). Together, these observations
474 suggest that ERM may be phosphorylated at the critical C-terminal threonine site by different
475 upstream pathways that can vary from endothelium to endothelium and from stimuli to stimuli.

476 We and others previously have demonstrated that several PKC isoforms - conventional,
477 unconventional and atypical—are likely to phosphorylate the C-terminal threonine residue of
478 ERM proteins (1, 35, 52, 67). Our data now demonstrate that PKC isoforms ζ , γ , ϵ , θ and
479 δ , which previously have been demonstrated to play roles in inflammation-induced changes in
480 endothelial permeability (16, 44, 53, 56, 61, 62, 70), participate in thrombin-induced ERM
481 phosphorylation at the C-terminal threonine site in human pulmonary EC (Figure 6). Moreover,
482 our data indicate that these isoforms may synergistically regulate both ERM threonine and MLC

483 phosphorylation (Fig. 6C, D). One of the key events in the signaling cascade triggered by
484 thrombin binding to PAR receptors is Ca^{2+} -dependent activation of PKC and Ca^{2+} /calmodulin-
485 dependent MLCK, which phosphorylates myosin light chain (MLC) (12, 37). RhoA and its
486 effector ROCK indirectly regulate MLCK activation and MLC phosphorylation and therefore
487 also mediate endothelial hyperpermeability in response to thrombin (8, 49, 64). The
488 RhoA/ROCK pathway is one of the downstream signals activated by PKC (8). Data
489 demonstrating that ERM are phosphorylated by PKC in response to thrombin prompted us to
490 examine the time-dependent phosphorylation status of individual ERM and whether ERM play a
491 role in MLC phosphorylation after thrombin. The effects of ERM siRNA treatment, either singly
492 or in combination, on the phosphorylated ERM and MLC phosphorylation before or after
493 thrombin treatment were examined. We discovered that all three proteins were phosphorylated;
494 however, knockdown of moesin alone or all three ERM proteins together significantly reduced
495 thrombin-induced ERM and MLC phosphorylation (0-90 minutes). In contrast, depletion of
496 radixin did not have any significant effect on MLC phosphorylation while slightly reducing
497 ERM threonine phosphorylation after thrombin. Depletion of ezrin partially attenuated thrombin-
498 induced ERM and MLC phosphorylation. Importantly, these data demonstrate differential roles
499 for the ERM proteins in response to thrombin, despite their structural similarities and reported
500 functional redundancy. These data also clearly suggest that moesin and to a lesser degree ezrin,
501 but not radixin, are critically involved in MLC phosphorylation after thrombin.

502 The underlying mechanism through which moesin and ezrin regulate MLC phosphorylation
503 remains to be determined. ERM proteins are known to activate the Rho signaling in cell adhesion
504 regulation via association with Rho regulator Rho GDP-dissociation inhibitor (GDI) (58). Our
505 data indicate that ERM may be upstream of MLC phosphorylation. Depletion of PKC isoforms

506 (Fig. 6A-D) indicated that PKC-dependent moesin and ezrin phosphorylation on regulatory C-
507 terminal threonine is involved in thrombin-induced RhoA activation and subsequent increased
508 MLC phosphorylation. In addition, phosphorylation of moesin or/and ezrin at sites other than C-
509 terminal threonine may contribute to this activation. For example, several additional sites have
510 been reported for ezrin (threonine 235, tyrosines 145 and 353) (36, 73), but the functional roles
511 of phosphorylation at these sites are still unclear. Interestingly, as we recently have been reported
512 (31), each ERM protein has a distinct binding ability toward the subunits (CSI β and MYPT) of
513 MLC phosphatase (MLCP), a type 1 protein phosphatase (PPase 1) that regulate reversible
514 phosphorylation of the MLC in intercellular gap formation and barrier dysfunction of EC. Our
515 data demonstrated that the catalytical subunit CSI β preferably bound to moesin, while the band
516 that corresponds to ezrin detected in CSI β immunoprecipitates is faint. In contrast, radixin did
517 not bind to CSI β , but strongly interacted with MLCP targeting subunit MYPT I. It is possible,
518 that in addition to RhoA activation after thrombin, moesin may inhibit MLCP function leading to
519 increased MLC phosphorylation. Our prior results indicated that MLCP play an important role in
520 barrier protection in EC (31). Radixin may regulate MLCP activation through binding to MYPT
521 I in S1P-induced barrier enhancement. Future studies will be needed to clarify the link between
522 PKC/ERM and Rho/ROCK/MLCP pathways in thrombin-induced formation of stress fibers and
523 increased endothelial permeability.

524 We next examined the role of ERM in thrombin-induced cytoskeletal changes. Thrombin
525 induces translocation of phosphorylated ERM from the cytoplasm to EC periphery during the
526 early stages of cells contraction and loss of monolayer integrity (Figure 11), which is consistent
527 with previous studies (1, 9, 35). Most importantly, our data again demonstrate differential roles
528 for the ERM proteins in response to thrombin. Moesin exerted a particularly prominent and

529 essential role in the promotion of EC barrier dysfunction by thrombin, while radixin appears to
530 have opposing effects. This observation is consistent with recent reports describing moesin
531 involvement in increased permeability induced by hypoxia and truncation of monocyte
532 chemoattractant protein 1 in the blood-brain barrier (25, 74) and AGE in human microvascular
533 EC (23, 68). Prior data obtained using knockout mice lacking individual ERM proteins largely
534 support the functional redundancy of the three ERM proteins (11, 32, 54). However recent
535 studies demonstrate differential biological functioning of these proteins. For example, ezrin and
536 moesin have distinct and critical functions in the T cell cortex during immunological synapse
537 formation (28). Moreover, ezrin, but not moesin, is phosphorylated on tyrosine in EGF-
538 challenged human A431 cells despite tyrosine 145 conservation in both proteins (17). In
539 addition, moesin has a non-redundant function in lymphocyte homeostasis (26). Our recent
540 findings also support the distinct biological roles of these proteins in agonist-mediated EC barrier
541 responses (1).

542 The observation that phosphorylated ERM is mostly localized to the peripheral area in EC
543 undergoing contraction after thrombin stimulation led us to examine the role of these proteins in
544 modulating permeability increases. We evaluated the role of ERM in thrombin-induced
545 hyperpermeability by measuring the TER in ERM depleted EC. The depletion of moesin alone or
546 triple ERM siRNA knockdown significantly attenuated the increase in permeability after
547 thrombin (Figure 8A, D and E). Ezrin knockdown also attenuated the decrease in TER induced
548 by thrombin, but to a lesser degree than moesin (Fig. 8C, E). In contrast, radixin depletion leads
549 to a slight increase in permeability during the early phase and delayed recovery during the later
550 phase of thrombin-mediated decreases in TER (Fig. 8B, E). These results suggest that ERM are
551 differentially involved in the development of thrombin-induced permeability with moesin and

552 ezrin promoting barrier permeability during the phase of active contraction (5-60 minutes of
553 treatment with thrombin). In contrast, despite the lower level of expression compare to moesin
554 and ezrin, radixin exerted a particularly prominent and essential role in the promotion of EC
555 barrier function in the restoration phase (60-120 minutes of treatment).

556 In EC, thrombin-induced activation of PAR₁ receptor initiate signaling through G_q- and
557 G_{12/13}-coupled Ca²⁺ mobilization, PKC and RhoA activation, and MAPK signaling (5, 7, 27). In
558 addition, thrombin transactivates PAR₂ through PAR₁ (48). We next used PAR₁ (TFLLR-NH₂),
559 PAR₂ (SLIGRL-NH₂) selective agonists and the PAR₁-specific blocking antibodies ATAP2 and
560 WEDE15 to determine the role of PARs in thrombin-induced threonine phosphorylation of
561 ERM. Our data indicate that thrombin primarily induces ERM threonine phosphorylation in
562 pulmonary EC by combined activation of both PAR₁ and PAR₂.

563

564 **Conclusion**

565 The present study demonstrates that thrombin induces PKC-dependent ERM
566 phosphorylation on a critical threonine residue (Ezrin-567, Radixin-564, Moesin-558) and
567 translocation of phosphorylated ERM to the EC periphery. ERM phosphorylation is mediated
568 by the combined actions of PAR₁ and PAR₂. Thrombin-induced barrier dysfunction in
569 pulmonary endothelium is associated with remodeling of the actin cytoskeleton that increases
570 permeability. ERM proteins are critically involved in the barrier-disruptive response induced in
571 the endothelium by thrombin and may modulate cytoskeletal changes and barrier
572 hyperpermeability via such intermediate signaling events as PKC mediated RhoA/ROCK-
573 dependent signaling. Our data demonstrate that depletion of either moesin alone, or of all three
574 ERM proteins, attenuates thrombin-induced F-actin cytoskeleton rearrangement, paracellular gap

575 formation, MLC phosphorylation and decrease in TER. In contrast, radixin depletion has the
576 opposite effect on barrier function. Based on these results and our prior data (1), we propose the
577 following model of ERM-dependent signaling in thrombin- and S1P-treated ECs (Fig. 14):
578 thrombin treatment induces PAR₁ and PAR₂-mediated C-terminal threonine phosphorylation
579 primarily of moesin and ezrin by PKC and PIP₂. Recently it has been reported that
580 phosphorylation of the RhoA activator - guanine nucleotide exchange factor p115RhoGEF by
581 PKC- α mediates TNF- α -induced RhoA activation and subsequent barrier dysfunction in mouse
582 brain microvascular endothelial cells (51). We hypothesize that PKC isoforms may
583 simultaneously phosphorylate both moesin and ezrin and p115RhoGEF. Activated moesin and
584 ezrin may displace RhoGDI from RhoA, allowing p115RhoGEF mediated RhoA activation by
585 GDP to GTP exchange. Increased intracellular concentration of Ca²⁺ activates MLCK. RhoA and
586 MLCK phosphorylate MLC, allowing EC contraction and reorganization of the cytoskeleton,
587 resulting in endothelial barrier dysfunction. In contrast, S1P induces S1PR1-mediated radixin
588 activation (primarily), resulting in Rac1 activation. Activated Rac1 via its downstream target
589 PAK1 induces actomyosin remodeling, including formation of a prominent cortical actin rim,
590 which stabilizes cell-cell junctions, peripheral accumulation of phosphorylated MLC, and
591 disappearance of central stress fibers, resulting in endothelial barrier enhancement. Thus, despite
592 their structural similarities and reported functional redundancy, the ERM proteins differentially
593 modulate thrombin-induced changes in lung EC cytoskeleton and permeability. These results
594 advance our mechanistic understanding of EC barrier regulation, identify the ERM family as
595 potential targets for therapeutic manipulation in this clinically important physiologic process and
596 extend previous knowledge about the involvement of PKC and ERM in endothelial barrier
597 regulation.

598 **Acknowledgments**

599 The authors are grateful to Drs. D. Fulton and S. Black from Georgia Health Sciences University
600 for help with moesin mutant preparation.

601

602 **Grants**

603 This work was supported by grants from the National Institutes of Health (NIH) grant HL58064,
604 HL88144 and HL101902.

605

606

607

608

609

610

611

612

613

614

615

616

617

618

619

620

621

622 **References**

- 623
- 624 1. **Adyshev DM, Moldobaeva NK, Elangovan VR, Garcia JG, and Dudek SM.**
625 Differential involvement of ezrin/radixin/moesin proteins in sphingosine 1-phosphate-induced
626 human pulmonary endothelial cell barrier enhancement. *Cellular signalling* 23: 2086-2096,
627 2011.
- 628 2. **Arpin M, Chirivino D, Naba A, and Zwaenepoel I.** Emerging role for ERM proteins in
629 cell adhesion and migration. *Cell adhesion & migration* 5: 199-206, 2011.
- 630 3. **Belkina NV, Liu Y, Hao JJ, Karasuyama H, and Shaw S.** LOK is a major ERM kinase
631 in resting lymphocytes and regulates cytoskeletal rearrangement through ERM phosphorylation.
632 *Proceedings of the National Academy of Sciences of the United States of America* 106: 4707-
633 4712, 2009.
- 634 4. **Berryman M, Franck Z, and Bretscher A.** Ezrin is concentrated in the apical microvilli
635 of a wide variety of epithelial cells whereas moesin is found primarily in endothelial cells.
636 *Journal of cell science* 105 (Pt 4): 1025-1043, 1993.
- 637 5. **Birukova AA, Birukov KG, Smurova K, Adyshev D, Kaibuchi K, Alieva I, Garcia**
638 **JG, and Verin AD.** Novel role of microtubules in thrombin-induced endothelial barrier
639 dysfunction. *Faseb J* 18: 1879-1890, 2004.
- 640 6. **Birukova AA, Smurova K, Birukov KG, Kaibuchi K, Garcia JG, and Verin AD.**
641 Role of Rho GTPases in thrombin-induced lung vascular endothelial cells barrier dysfunction.
642 *Microvascular research* 67: 64-77, 2004.
- 643 7. **Bogatcheva NV, Garcia JG, and Verin AD.** Molecular mechanisms of thrombin-
644 induced endothelial cell permeability. *Biochemistry* 67: 75-84, 2002.
- 645 8. **Bogatcheva NV, and Verin AD.** The role of cytoskeleton in the regulation of vascular
646 endothelial barrier function. *Microvascular research* 76: 202-207, 2008.
- 647 9. **Bogatcheva NV, Zemskova MA, Gorshkov BA, Kim KM, Daglis GA, Poirier C, and**
648 **Verin AD.** Ezrin, radixin, and moesin are phosphorylated in response to 2-methoxyestradiol and
649 modulate endothelial hyperpermeability. *American journal of respiratory cell and molecular*
650 *biology* 45: 1185-1194, 2011.
- 651 10. **Cant SH, and Pitcher JA.** G protein-coupled receptor kinase 2-mediated
652 phosphorylation of ezrin is required for G protein-coupled receptor-dependent reorganization of
653 the actin cytoskeleton. *Molecular biology of the cell* 16: 3088-3099, 2005.
- 654 11. **Doi Y, Itoh M, Yonemura S, Ishihara S, Takano H, Noda T, and Tsukita S.** Normal
655 development of mice and unimpaired cell adhesion/cell motility/actin-based cytoskeleton
656 without compensatory up-regulation of ezrin or radixin in moesin gene knockout. *The Journal of*
657 *biological chemistry* 274: 2315-2321, 1999.
- 658 12. **Dudek SM, and Garcia JG.** Cytoskeletal regulation of pulmonary vascular
659 permeability. *Journal of Applied Physiology* 91: 1487-1500, 2001.
- 660 13. **Elbashir SM, Harborth J, Lendeckel W, Yalcin A, Weber K, and Tuschl T.**
661 Duplexes of 21-nucleotide RNAs mediate RNA interference in cultured mammalian cells.
662 *Nature* 411: 494-498, 2001.
- 663 14. **Fehon RG, McClatchey AI, and Bretscher A.** Organizing the cell cortex: the role of
664 ERM proteins. *Nature reviews* 11: 276-287, 2010.
- 665 15. **Fievet BT, Gautreau A, Roy C, Del Maestro L, Mangeat P, Louvard D, and Arpin**
666 **M.** Phosphoinositide binding and phosphorylation act sequentially in the activation mechanism
667 of ezrin. *The Journal of cell biology* 164: 653-659, 2004.

- 668 16. **Fleegal MA, Hom S, Borg LK, and Davis TP.** Activation of PKC modulates blood-
669 brain barrier endothelial cell permeability changes induced by hypoxia and posthypoxic
670 reoxygenation. *Am J Physiol Heart Circ Physiol* 289: H2012-2019, 2005.
- 671 17. **Franck Z, Gary R, and Bretscher A.** Moesin, like ezrin, colocalizes with actin in the
672 cortical cytoskeleton in cultured cells, but its expression is more variable. *Journal of cell science*
673 105 (Pt 1): 219-231, 1993.
- 674 18. **Garcia JG, Davis HW, and Patterson CE.** Regulation of endothelial cell gap formation
675 and barrier dysfunction: role of myosin light chain phosphorylation. *Journal of cellular*
676 *physiology* 163: 510-522, 1995.
- 677 19. **Garcia JG, Liu F, Verin AD, Birukova A, Dechert MA, Gerthoffer WT, Bamberg**
678 **JR, and English D.** Sphingosine 1-phosphate promotes endothelial cell barrier integrity by Edg-
679 dependent cytoskeletal rearrangement. *The Journal of clinical investigation* 108: 689-701, 2001.
- 680 20. **Garcia JG, Siflinger-Birnboim A, Bizios R, Del Vecchio PJ, Fenton JW, 2nd, and**
681 **Malik AB.** Thrombin-induced increase in albumin permeability across the endothelium. *Journal*
682 *of cellular physiology* 128: 96-104, 1986.
- 683 21. **Gautreau A, Louvard D, and Arpin M.** Morphogenic effects of ezrin require a
684 phosphorylation-induced transition from oligomers to monomers at the plasma membrane. *The*
685 *Journal of cell biology* 150: 193-203, 2000.
- 686 22. **Grand RJ, Turnell AS, and Grabham PW.** Cellular consequences of thrombin-
687 receptor activation. *The Biochemical journal* 313 (Pt 2): 353-368, 1996.
- 688 23. **Guo X, Wang L, Chen B, Li Q, Wang J, Zhao M, Wu W, Zhu P, Huang X, and**
689 **Huang Q.** ERM protein moesin is phosphorylated by advanced glycation end products and
690 modulates endothelial permeability. *Am J Physiol Heart Circ Physiol* 297: H238-246, 2009.
- 691 24. **Hayashi K, Yonemura S, Matsui T, and Tsukita S.** Immunofluorescence detection of
692 ezrin/radixin/moesin (ERM) proteins with their carboxyl-terminal threonine phosphorylated in
693 cultured cells and tissues. *Journal of cell science* 112 (Pt 8): 1149-1158, 1999.
- 694 25. **Hicks K, O'Neil RG, Dubinsky WS, and Brown RC.** TRPC-mediated actin-myosin
695 contraction is critical for BBB disruption following hypoxic stress. *American journal of*
696 *physiology* 298: C1583-1593, 2010.
- 697 26. **Hirata T, Nomachi A, Tohya K, Miyasaka M, Tsukita S, Watanabe T, and**
698 **Narumiya S.** Moesin-deficient mice reveal a non-redundant role for moesin in lymphocyte
699 homeostasis. *International immunology* 24: 705-717, 2012.
- 700 27. **Holinstat M, Mehta D, Kozasa T, Minshall RD, and Malik AB.** Protein kinase
701 Calpha-induced p115RhoGEF phosphorylation signals endothelial cytoskeletal rearrangement.
702 *The Journal of biological chemistry* 278: 28793-28798, 2003.
- 703 28. **Ilani T, Khanna C, Zhou M, Veenstra TD, and Bretscher A.** Immune synapse
704 formation requires ZAP-70 recruitment by ezrin and CD43 removal by moesin. *The Journal of*
705 *cell biology* 179: 733-746, 2007.
- 706 29. **Ivetic A, and Ridley AJ.** Ezrin/radixin/moesin proteins and Rho GTPase signalling in
707 leucocytes. *Immunology* 112: 165-176, 2004.
- 708 30. **Johnson MW, Miyata H, and Vinters HV.** Ezrin and moesin expression within the
709 developing human cerebrum and tuberous sclerosis-associated cortical tubers. *Acta*
710 *neuropathologica* 104: 188-196, 2002.
- 711 31. **Kim KM, Csontos C, Czikora I, Fulton D, Umopathy NS, Olah G, and Verin AD.**
712 Molecular characterization of myosin phosphatase in endothelium. *Journal of cellular*
713 *physiology* 227: 1701-1708, 2012.

- 714 32. **Kitajiri S, Fukumoto K, Hata M, Sasaki H, Katsuno T, Nakagawa T, Ito J, Tsukita**
715 **S, and Tsukita S.** Radixin deficiency causes deafness associated with progressive degeneration
716 of cochlear stereocilia. *The Journal of cell biology* 166: 559-570, 2004.
- 717 33. **Knezevic N, Roy A, Timblin B, Konstantoulaki M, Sharma T, Malik AB, and Mehta**
718 **D.** GDI-1 phosphorylation switch at serine 96 induces RhoA activation and increased endothelial
719 permeability. *Molecular and cellular biology* 27: 6323-6333, 2007.
- 720 34. **Konstantoulaki M, Kouklis P, and Malik AB.** Protein kinase C modifications of VE-
721 cadherin, p120, and beta-catenin contribute to endothelial barrier dysregulation induced by
722 thrombin. *Am J Physiol Lung Cell Mol Physiol* 285: L434-442, 2003.
- 723 35. **Koss M, Pfeiffer GR, 2nd, Wang Y, Thomas ST, Yerukhimovich M, Gaarde WA,**
724 **Doerschuk CM, and Wang Q.** Ezrin/radixin/moesin proteins are phosphorylated by TNF-alpha
725 and modulate permeability increases in human pulmonary microvascular endothelial cells. *J*
726 *Immunol* 176: 1218-1227, 2006.
- 727 36. **Krieg J, and Hunter T.** Identification of the two major epidermal growth factor-induced
728 tyrosine phosphorylation sites in the microvillar core protein ezrin. *The Journal of biological*
729 *chemistry* 267: 19258-19265, 1992.
- 730 37. **Kumar P, Shen Q, Pivetti CD, Lee ES, Wu MH, and Yuan SY.** Molecular
731 mechanisms of endothelial hyperpermeability: implications in inflammation. *Expert reviews in*
732 *molecular medicine* 11: e19, 2009.
- 733 38. **Li Z, Liu YH, Xue YX, Liu LB, and Wang P.** Signal mechanisms underlying low-dose
734 endothelial monocyte-activating polypeptide-II-induced opening of the blood-tumor barrier. *J*
735 *Mol Neurosci* 48: 291-301, 2012 .
- 736 39. **Martiny-Baron G, Kazanietz MG, Mischak H, Blumberg PM, Kochs G, Hug H,**
737 **Marme D, and Schachtele C.** Selective inhibition of protein kinase C isozymes by the
738 indolocarbazole Go 6976. *The Journal of biological chemistry* 268: 9194-9197, 1993.
- 739 40. **Matsui T, Maeda M, Doi Y, Yonemura S, Amano M, Kaibuchi K, Tsukita S, and**
740 **Tsukita S.** Rho-kinase phosphorylates COOH-terminal threonines of ezrin/radixin/moesin
741 (ERM) proteins and regulates their head-to-tail association. *The Journal of cell biology* 140: 647-
742 657, 1998.
- 743 41. **Matsui T, Yonemura S, Tsukita S, and Tsukita S.** Activation of ERM proteins in vivo
744 by Rho involves phosphatidylinositol 4-phosphate 5-kinase and not ROCK kinases. *Curr Biol* 9:
745 1259-1262, 1999.
- 746 42. **McLaughlin JN, Shen L, Holinstat M, Brooks JD, Dibenedetto E, and Hamm HE.**
747 Functional selectivity of G protein signaling by agonist peptides and thrombin for the protease-
748 activated receptor-1. *The Journal of biological chemistry* 280: 25048-25059, 2005.
- 749 43. **Mehta D, and Malik AB.** Signaling mechanisms regulating endothelial permeability.
750 *Physiological reviews* 86: 279-367, 2006.
- 751 44. **Minshall RD, Vandenbroucke EE, Holinstat M, Place AT, Tirupathi C, Vogel SM,**
752 **van Nieuw Amerongen GP, Mehta D, and Malik AB.** Role of protein kinase C ζ in
753 thrombin-induced RhoA activation and inter-endothelial gap formation of human dermal
754 microvessel endothelial cell monolayers. *Microvascular research* 80: 240-249, 2010.
- 755 45. **Moy AB, Blackwell K, and Kamath A.** Differential effects of histamine and thrombin
756 on endothelial barrier function through actin-myosin tension. *Am J Physiol Heart Circ Physiol*
757 282: H21-29, 2002.
- 758 46. **Neisch AL, and Fehon RG.** Ezrin, Radixin and Moesin: key regulators of membrane-
759 cortex interactions and signaling. *Current opinion in cell biology* 23: 377-382, 2011.

- 760 47. **Ng T, Parsons M, Hughes WE, Monypenny J, Zicha D, Gautreau A, Arpin M,**
761 **Gschmeissner S, Verveer PJ, Bastiaens PI, and Parker PJ.** Ezrin is a downstream effector of
762 trafficking PKC-integrin complexes involved in the control of cell motility. *The EMBO journal*
763 20: 2723-2741, 2001.
- 764 48. **O'Brien PJ, Prevost N, Molino M, Hollinger MK, Woolkalis MJ, Woulfe DS, and**
765 **Brass LF.** Thrombin responses in human endothelial cells. Contributions from receptors other
766 than PAR1 include the transactivation of PAR2 by thrombin-cleaved PAR1. *The Journal of*
767 *biological chemistry* 275: 13502-13509, 2000.
- 768 49. **Patil SB, and Bitar KN.** RhoA- and PKC-alpha-mediated phosphorylation of MYPT and
769 its association with HSP27 in colonic smooth muscle cells. *Am J Physiol Gastrointest Liver*
770 *Physiol* 290: G83-95, 2006.
- 771 50. **Pearson MA, Reczek D, Bretscher A, and Karplus PA.** Structure of the ERM protein
772 moesin reveals the FERM domain fold masked by an extended actin binding tail domain. *Cell*
773 101: 259-270, 2000.
- 774 51. **Peng J, He F, Zhang C, Deng X, and Yin F.** Protein kinase C-alpha signals
775 P115RhoGEF phosphorylation and RhoA activation in TNF-alpha-induced mouse brain
776 microvascular endothelial cell barrier dysfunction. *Journal of neuroinflammation* 8: 28, 2011.
- 777 52. **Pietromonaco SF, Simons PC, Altman A, and Elias L.** Protein kinase C-theta
778 phosphorylation of moesin in the actin-binding sequence. *The Journal of biological chemistry*
779 273: 7594-7603, 1998.
- 780 53. **Rigor RR, Beard RS, Jr., Litovka OP, and Yuan SY.** Interleukin-1beta-induced barrier
781 dysfunction is signaled through PKC-theta in human brain microvascular endothelium. *American*
782 *journal of physiology* 302: C1513-1522, 2012.
- 783 54. **Saotome I, Curto M, and McClatchey AI.** Ezrin is essential for epithelial organization
784 and villus morphogenesis in the developing intestine. *Developmental cell* 6: 855-864, 2004.
- 785 55. **Schaphorst KL, Pavalko FM, Patterson CE, and Garcia JG.** Thrombin-mediated
786 focal adhesion plaque reorganization in endothelium: role of protein phosphorylation. *American*
787 *journal of respiratory cell and molecular biology* 17: 443-455, 1997.
- 788 56. **Sonobe Y, Takeuchi H, Kataoka K, Li H, Jin S, Mimuro M, Hashizume Y, Sano Y,**
789 **Kanda T, Mizuno T, and Suzumura A.** Interleukin-25 expressed by brain capillary endothelial
790 cells maintains blood-brain barrier function in a protein kinase Cepsilon-dependent manner. *The*
791 *Journal of biological chemistry* 284: 31834-31842, 2009.
- 792 57. **Srivastava J, Elliott BE, Louvard D, and Arpin M.** Src-dependent ezrin
793 phosphorylation in adhesion-mediated signaling. *Molecular biology of the cell* 16: 1481-1490,
794 2005.
- 795 58. **Takahashi K, Sasaki T, Mammoto A, Takaishi K, Kameyama T, Tsukita S, and**
796 **Takai Y.** Direct interaction of the Rho GDP dissociation inhibitor with ezrin/radixin/moesin
797 initiates the activation of the Rho small G protein. *The Journal of biological chemistry* 272:
798 23371-23375, 1997.
- 799 59. **ten Klooster JP, Jansen M, Yuan J, Oorschot V, Begthel H, Di Giacomo V, Colland**
800 **F, de Koning J, Maurice MM, Hornbeck P, and Clevers H.** Mst4 and Ezrin induce brush
801 borders downstream of the Lkb1/Strad/Mo25 polarization complex. *Developmental cell* 16: 551-
802 562, 2009.
- 803 60. **Tinsley JH, De Lanerolle P, Wilson E, Ma W, and Yuan SY.** Myosin light chain
804 kinase transference induces myosin light chain activation and endothelial hyperpermeability.
805 *American journal of physiology* 279: C1285-1289, 2000.

- 806 61. **Tinsley JH, Teasdale NR, and Yuan SY.** Involvement of PKCdelta and PKD in
807 pulmonary microvascular endothelial cell hyperpermeability. *American journal of physiology*
808 286: C105-111, 2004.
- 809 62. **Titchenell PM, Lin CM, Keil JM, Sundstrom JM, Smith CD, and Antonetti DA.**
810 Novel atypical PKC inhibitors prevent vascular endothelial growth factor-induced blood-retinal
811 barrier dysfunction. *The Biochemical journal* 446: 455-467, 2012.
- 812 63. **Toullec D, Pianetti P, Coste H, Bellevergue P, Grand-Perret T, Ajakane M, Baudet**
813 **V, Boissin P, Boursier E, Loriolle F, and et al.** The bisindolylmaleimide GF 109203X is a
814 potent and selective inhibitor of protein kinase C. *The Journal of biological chemistry* 266:
815 15771-15781, 1991.
- 816 64. **van Nieuw Amerongen GP, van Delft S, Vermeer MA, Collard JG, and van**
817 **Hinsbergh VW.** Activation of RhoA by thrombin in endothelial hyperpermeability: role of Rho
818 kinase and protein tyrosine kinases. *Circulation research* 87: 335-340, 2000.
- 819 65. **Verin AD, Birukova A, Wang P, Liu F, Becker P, Birukov K, and Garcia JG.**
820 Microtubule disassembly increases endothelial cell barrier dysfunction: role of MLC
821 phosphorylation. *Am J Physiol Lung Cell Mol Physiol* 281: L565-574, 2001.
- 822 66. **Vu TK, Hung DT, Wheaton VI, and Coughlin SR.** Molecular cloning of a functional
823 thrombin receptor reveals a novel proteolytic mechanism of receptor activation. *Cell* 64: 1057-
824 1068, 1991.
- 825 67. **Wald FA, Oriolo AS, Mashukova A, Fregien NL, Langshaw AH, and Salas PJ.**
826 Atypical protein kinase C (iota) activates ezrin in the apical domain of intestinal epithelial cells.
827 *Journal of cell science* 121: 644-654, 2008.
- 828 68. **Wang J, Liu H, Chen B, Li Q, Huang X, Wang L, Guo X, and Huang Q.**
829 RhoA/ROCK-dependent moesin phosphorylation regulates AGE-induced endothelial cellular
830 response. *Cardiovascular diabetology* 11: 7, 2012.
- 831 69. **Wilkinson SE, Parker PJ, and Nixon JS.** Isoenzyme specificity of
832 bisindolylmaleimides, selective inhibitors of protein kinase C. *The Biochemical journal* 294 (Pt
833 2): 335-337, 1993.
- 834 70. **Willis CL, Meske DS, and Davis TP.** Protein kinase C activation modulates reversible
835 increase in cortical blood-brain barrier permeability and tight junction protein expression during
836 hypoxia and posthypoxic reoxygenation. *J Cereb Blood Flow Metab* 30: 1847-1859, 2010.
- 837 71. **Wu KL, Khan S, Lakhe-Reddy S, Jarad G, Mukherjee A, Obejero-Paz CA,**
838 **Konieczkowski M, Sedor JR, and Schelling JR.** The NHE1 Na⁺/H⁺ exchanger recruits
839 ezrin/radixin/moesin proteins to regulate Akt-dependent cell survival. *The Journal of biological*
840 *chemistry* 279: 26280-26286, 2004.
- 841 72. **Wysolmerski RB, and Lagunoff D.** Regulation of permeabilized endothelial cell
842 retraction by myosin phosphorylation. *The American journal of physiology* 261: C32-40, 1991.
- 843 73. **Yang HS, and Hinds PW.** Increased ezrin expression and activation by CDK5
844 coincident with acquisition of the senescent phenotype. *Molecular cell* 11: 1163-1176, 2003.
- 845 74. **Yao Y, and Tsirka SE.** Truncation of monocyte chemoattractant protein 1 by plasmin
846 promotes blood-brain barrier disruption. *Journal of cell science* 124: 1486-1495, 2011.
- 847
848
849

851 **Figure Legends**

852 **Figure 1. Relative quantity of moesin (MSN), ezrin (EZR), and radixin (RDX) mRNA in**
853 **HPAEC.** Total RNA was isolated from human pulmonary artery endothelial cells (HPAEC) and
854 quantitative real-time reverse transcriptase-polymerase chain reaction (qRT-PCR) was performed
855 using target gene specific primers and probes and the relative amounts expressed using standard
856 curve method as described in Methods. Each value represents the mean of triplicates.

857
858 **Figure 2. Time-dependent effects of thrombin on threonine phosphorylation of ERM. (A)**
859 Confluent HPAEC were treated either with control vehicle or thrombin (0.5 U/ml) for the
860 indicated times, and phosphorylated ERM (phospho-Ezrin (Thr567)/Radixin (Thr564)/Moesin
861 (Thr558) was detected via immunoblotting. (B) The bar graph represents relative densitometry.
862 Data are presented as fold changes in phosphorylated ERM over vehicle-treated control and
863 expressed as means \pm S.E. from three independent experiments. * $P < 0.05$ vs. unstimulated
864 control.

865
866 **Figure 3. Thrombin-induced ERM phosphorylation requires activation of PKC.** HPAEC
867 were pretreated with either control vehicle or the following inhibitors: PKC inhibitors Ro-31-
868 7549 (10 μ M, A, C) for 30 min, bisindolylmaleimide (BIM, 1 μ M, C) for 30 min, Go6976 (1
869 μ M, C) for 1 h, Ca(2+) chelator BAPTA-AM (25 μ M, A) for 1 h, p38 kinase inhibitor
870 SB203580 (20 μ M, A, B) for 30 min, Rho kinase inhibitors Y-27632 (10 μ M, A, B) for 1 h and
871 H-1152 (3 μ M, B) for 1 h, PI3 Kinase inhibitor LY294002 (10 μ M, A) for 1 hr. EC were then
872 stimulated with EBM-2 medium alone or thrombin (0.5 U/ml) for the indicated time.
873 Phosphorylation of ERM proteins and MLC were analyzed by immunoblotting of cell lysates

874 with phospho-ERM (as in Fig. 2) or di-phospho-MLC (Thr18/Ser19) specific Abs. GAPDH or β -
875 actin Abs were used as a normalization control. Rearranged lanes from the same blot are outlined
876 by vertical dotted line. Results of scanning densitometry of Western blots are shown as fold
877 changes of ERM or MLC phosphorylation relative to vehicle treated EC stimulated by thrombin.
878 Results are representative of 3-6 independent experiments. Values are means \pm S.E. *,
879 significantly different from cells treated with vehicle ($p < 0.05$); **, significantly different from
880 cells stimulated with thrombin ($p < 0.05$).

881
882 **Figure 4. Effects of thrombin on phosphorylation of PKC isoforms in HPAEC.** Confluent
883 HPAEC were treated either with control vehicle or thrombin (0.5U/ml) for the indicated times,
884 and phosphorylated PKC β (A), PKC γ (B), PKC ϵ (C), PKC ζ (D), PKC θ (E), and PKC δ (F) were
885 detected via immunoblotting. Bar graphs represent relative densitometry of fold changes in
886 phosphorylated PKC isoforms after thrombin relative to vehicle-treated control and expressed as
887 means \pm S.E. from three independent experiments. *, significantly different from cells treated
888 with EBM-2 ($p < 0.05$); #, significantly different from cells treated with EBM-2 ($p < 0.01$).

889
890 **Figure 5. Depletion of PKC isoforms by siRNA.** PKC ϵ (A) and PKC γ (B) depletion were
891 induced by specific siRNA duplexes and assessed for silencing effects by immunoblotting with
892 appropriate Ab, as compared with treatment with nonspecific (ns) siRNA. Immunoblotting with
893 β -actin Ab was used as a normalization control. Rearranged lanes from the same blot are outlined
894 by vertical dotted line. Quantitative analysis of protein expression was performed by scanning
895 densitometry and expressed in relative density units (RDU). Results are means \pm S.E. for three

896 independent experiments. #, significant difference ($p < 0.01$) when compared with cells treated
897 with ns siRNA.

898

899 **Figure 6. Depletion of PKC isoforms inhibits thrombin-induced ERM and MLC**

900 **phosphorylation.** Confluent HPAEC were incubated with non-specific, PKC β I-, PKC ζ -, PKC θ -

901 , PKC δ -, PKC γ - and PKC ϵ - specific siRNA (A) or with non-specific, combinations of PKC δ -

902 and PKC ϵ -, combinations of PKC γ - , PKC δ - and PKC ϵ - and combinations of PKC β I - , PKC θ -

903 and PKC ζ - specific siRNAs (C) as described in Methods, and then stimulated by thrombin (0.5

904 U/ml, 5 min) or vehicle. Total lysates were analyzed by immunoblotting for phospho-ERM or di-

905 phospho-MLC (Thr18/Ser19). Immunoblotting with β -tubulin Ab was used as a normalization

906 control. Rearranged lanes from the same blot are outlined by vertical dotted line. (B, D, E) The

907 bar graphs represent relative densitometry of fold changes in phosphorylated ERM and MLC

908 after thrombin relative to vehicle-treated control. Results are means \pm S.E. of four independent

909 experiments. *, significantly different from cells treated with ns siRNA without thrombin ($p <$

910 0.01); #, significantly different from cells treated with ns siRNA without thrombin ($p < 0.05$). **,

911 significantly different from cells treated with ns siRNA and thrombin ($p < 0.05$).

912

913 **Figure 7. Effects of ERM depletion on thrombin-induced ERM and MLC phosphorylation.**

914 Confluent HPAEC were incubated with non-specific, moesin- (panel A), radixin- (panel B),

915 ezrin-specific (panel C) or combined siRNAs for ezrin, radixin, and moesin (panel D) as

916 described in Methods then stimulated by thrombin (0.5 U/ml, 5 min) or vehicle. Total lysates

917 were analyzed by immunoblotting with phospho-ERM or di-phospho-MLC (Thr18/Ser19) Abs.

918 Immunoblotting with β -tubulin Ab was used as a normalization control. The bar graphs

919 represents relative densitometry of fold changes in phosphorylated ERM and MLC after
920 thrombin relative to vehicle-treated control. Results are means \pm S.E. of three independent
921 experiments. * $p < 0.05$, compared with corresponding pretreatment vehicle control.

922 **Figure 8. Effects of ERM depletion on thrombin-induced endothelial barrier**
923 **hyperpermeability.** EC grown in chambers on gold microelectrodes were transfected with
924 siRNA for moesin (panel A), radixin (panel B), ezrin (panel C), combined siRNAs for ezrin,
925 radixin, and moesin (panel D), or treated with nonspecific (ns) siRNA, as described in Methods
926 and used for transendothelial electrical resistance (TER) measurements. At time = 0, cells were
927 stimulated with thrombin (0.5 U/ml) or vehicle control. Shown are pooled data of 5 independent
928 experiments. The bar graph (E) depicts pooled TER data ($n = 5$) as maximal value of normalized
929 TER elevation above base line achieved within 30 min \pm S.E. *, significantly different from cells
930 treated with ns siRNA reagent without thrombin ($p < 0.05$); **, significantly different from
931 control cells stimulated with thrombin ($p < 0.05$).

932
933 **Figure 9. Effects of PAR₁ blocking antibodies on thrombin-induced ERM phosphorylation.**
934 (A) HPAEC were pretreated for 1 hour with either control vehicle or the PAR₁ blocking Abs
935 ATAP2 (25 μ g/ml) or WEDE15 (25 μ g/ml) or with combination of ATAP2 and WEDE15, then
936 stimulated by thrombin (0.5 U/ml, 5 min) or vehicle. Total lysates were analyzed by
937 immunoblotting for phospho-ERM. Immunoblotting with β -actin Ab was used as a
938 normalization control. (B) The bar graph represents relative densitometry of fold changes in
939 phosphorylated ERM after thrombin relative to vehicle-treated control. Results are means \pm S.E.
940 of four independent experiments. *, significantly different from cells treated with ns siRNA
941 without S1P ($p < 0.05$); #, significantly different from cells treated with ns siRNA without

942 thrombin ($p < 0.01$). **, significantly different from cells treated with ns siRNA and thrombin (p
943 < 0.05).

944

945 **Figure 10. Effects of PAR₁ and PAR₂ selective agonists on thrombin-induced ERM**

946 **phosphorylation.** (A) EC were pretreated for 5 minutes with thrombin (0.5 U/ml), PAR₁

947 selective agonist TFLLR-NH₂ (50 μM), PAR₂ selective agonist SLIGRL-NH₂ (50 μM) or

948 combination of TFLLR-NH₂ and SLIGRL-NH₂. Pretreatment with vehicle and reversed amino

949 acid sequence peptides RLLFT-NH₂ and LRGILS-NH₂ used as controls. (B) The bar graph

950 represents relative densitometry of fold changes in phosphorylated ERM after thrombin, TFLLR-

951 NH₂ or SLIGRL-NH₂ relative to vehicle-treated control. Results are means ± S.E. of three

952 independent experiments. * $p < 0.05$, compared with corresponding pretreatment controls.

953

954 **Figure 11. Distribution of phospho-ERM in EC after thrombin.** EC grown on glass cover

955 slips and treated with 0.5 U/ml thrombin for indicated time (images b-e) or non treated control

956 cells (image a) were subjected to immunofluorescent staining with anti-phospho-ERM Ab. The

957 phospho-ERM signal is very weak in quiescent monolayers and is evident only in spike-like

958 structures in cell-cell border areas (image a, arrow 1). Threonine-phosphorylated ERM proteins

959 predominantly localized to the periphery of ECs following thrombin stimulation (5-15 min,

960 images b,c, arrow 2) and also are detectable in peripheral spike-like structures (image b, arrow

961 1). After 1-2 hrs phosphorylated ERM localized in spike-like structures characteristic of

962 quiescent cells and in cytoplasm (images d,e). Images are representative of 3 independent

963 experiments. Scale bar = 10 μm.

964

965 **Figure 12. Effects of ERM depletion on thrombin-induced cytoskeletal remodeling.** HPAEC
966 grown on glass cover slips were incubated with siRNA to ezrin, radixin, moesin, or combination
967 of siRNAs to all three proteins, or treated with non-specific siRNA duplex as described in
968 Methods followed by thrombin treatment (0.5 U/ml, 5 min). ECs were subjected to double
969 immunofluorescent staining with Texas Red phalloidin to visualize F-actin (panels A and B,
970 upper images) and anti-pp-MLC Ab (Panels A and B, bottom images). Incubation with siRNA
971 to moesin (g, h) and combined siRNAs to ezrin, radixin, and moesin (o, p) almost completely
972 abolishes thrombin-induced F-actin stress fiber and gap formation and MLC phosphorylation
973 compared with control (nsRNA) incubation (c, d, arrows). In contrast, pretreatment with siRNA
974 to radixin slightly *enhances* the thickness of stress fibers and MLC phosphorylation (k, l, arrows)
975 compared with incubation with nsRNA. Bar = 10 μ M. Images are representative of three
976 independent experiments.

977

978 **Figure 13. Effects of overexpression of the phosphorylation-deficient mutant of moesin**
979 **(Thr558Ala) on thrombin-induced cytoskeletal remodeling.** (A) ECs were transfected with
980 empty vector (control), V5 tagged wild-type or mutant moesin, which were then detected via
981 immunoblotting with V5 Ab. Results of scanning densitometry of Western blots are shown as %
982 of moesin relative to control. Immunoblotting with β -actin Ab was used as a normalization
983 control. (B) After transfection with vectors expressing moesin (wild-type or mutant) tagged with
984 V5, EC were grown on glass cover slips as described in Methods followed by thrombin treatment
985 (0.5 U/ml, 5 min). ECs were subjected to double immunofluorescent staining with Texas Red
986 phalloidin to visualize F-actin (panels B and C, upper images) and V5 Ab (Panels B and C,
987 bottom images). Overexpression with mutant moesin abolishes thrombin-induced F-actin stress

988 fibers and induces cortical actin formation (panel C, image g) compared to EC overexpressed
989 with wild type moesin (panel C, image c). Arrow indicates cell transfected with mutant moesin
990 EC (panel C, image g). Images are representative of three independent experiments. Scale bar =
991 10 μm .

992

993 **Figure 14. Proposed model of ERM-dependent signaling in thrombin- and S1P-challenged**
994 **lung endothelium (see explanation in Conclusion).**

995

996

997

Figure 1

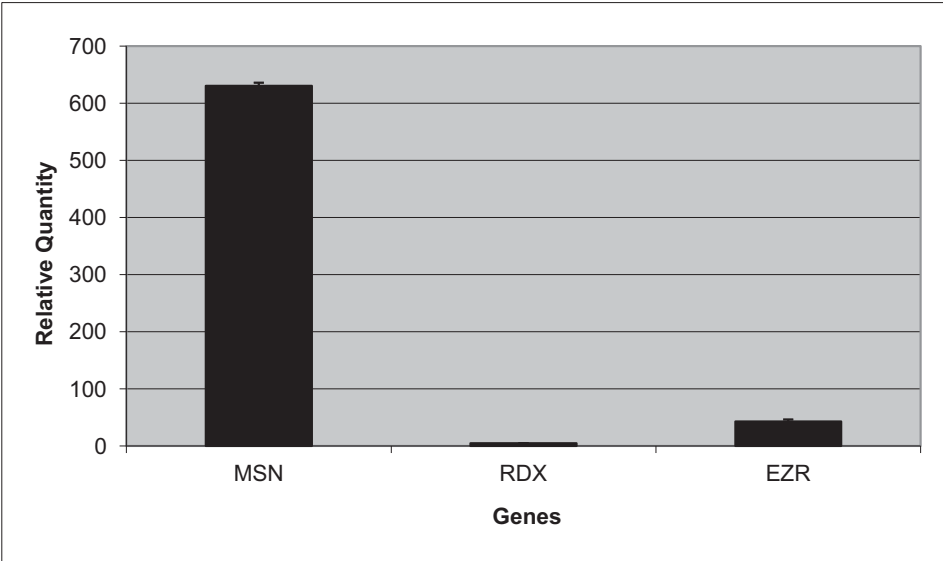


Figure 2

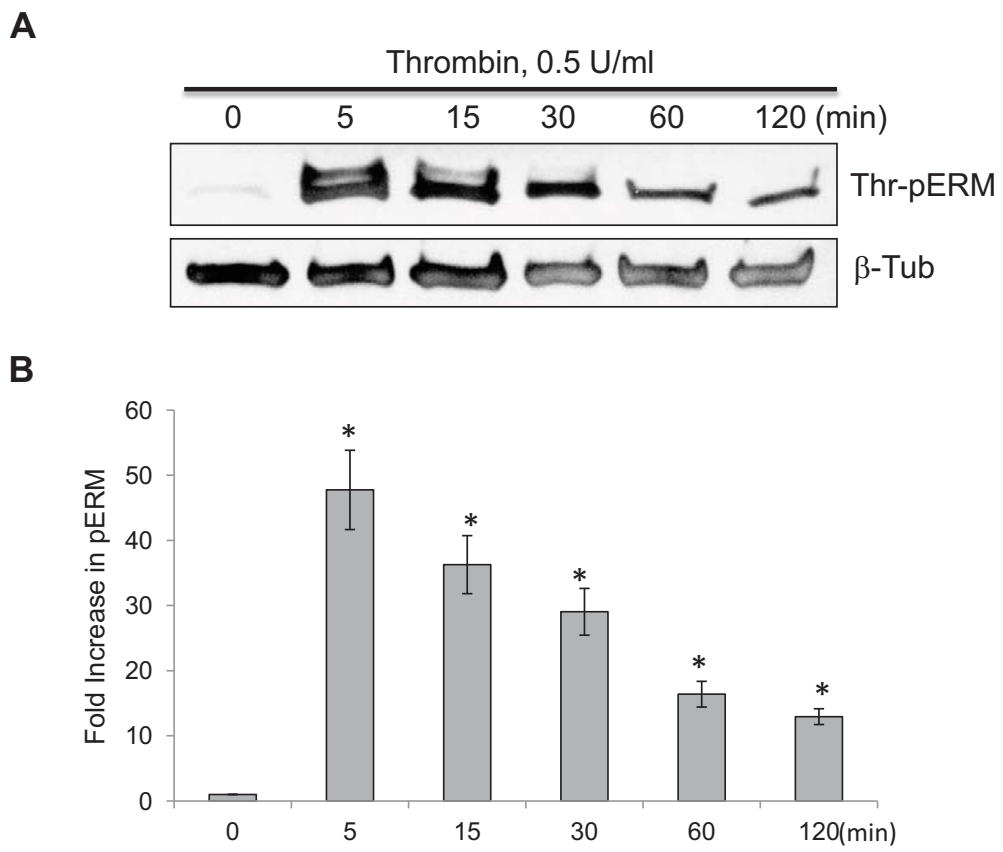


Figure 3A

A

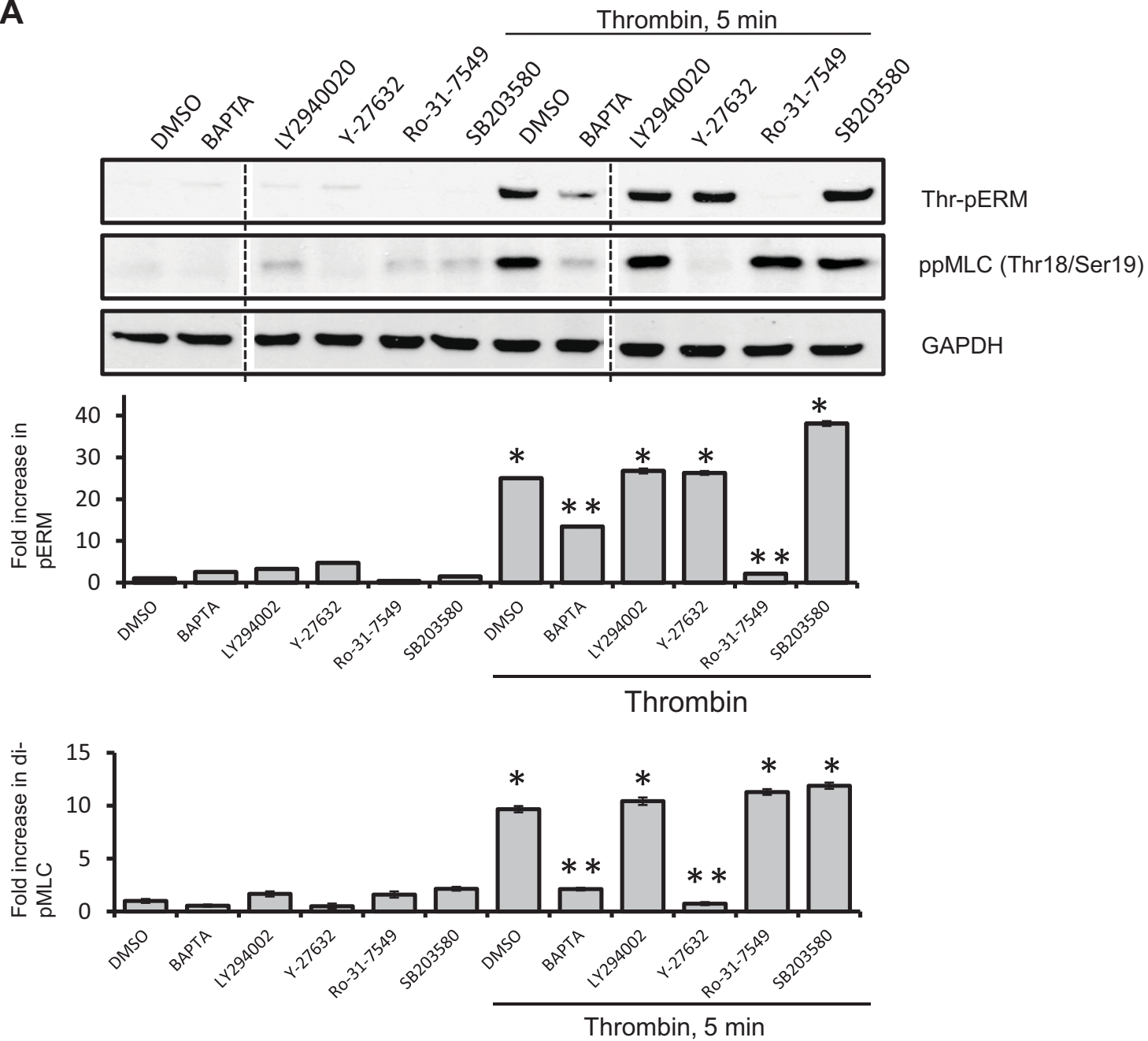


Figure 3B

B

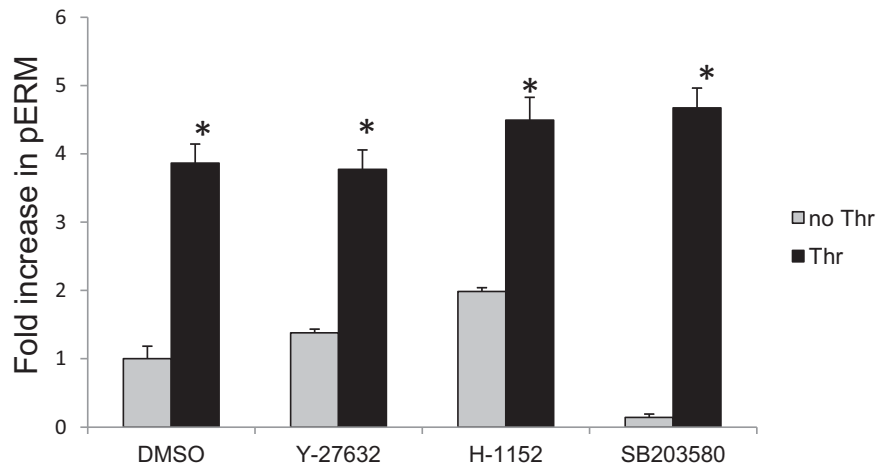
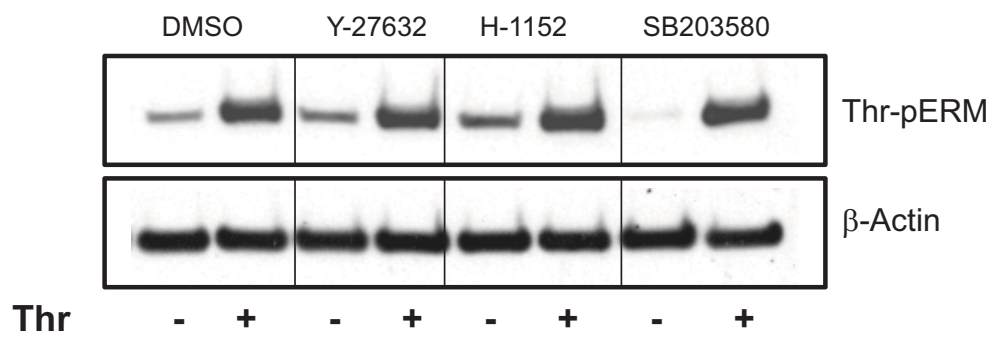


Figure 3C

C

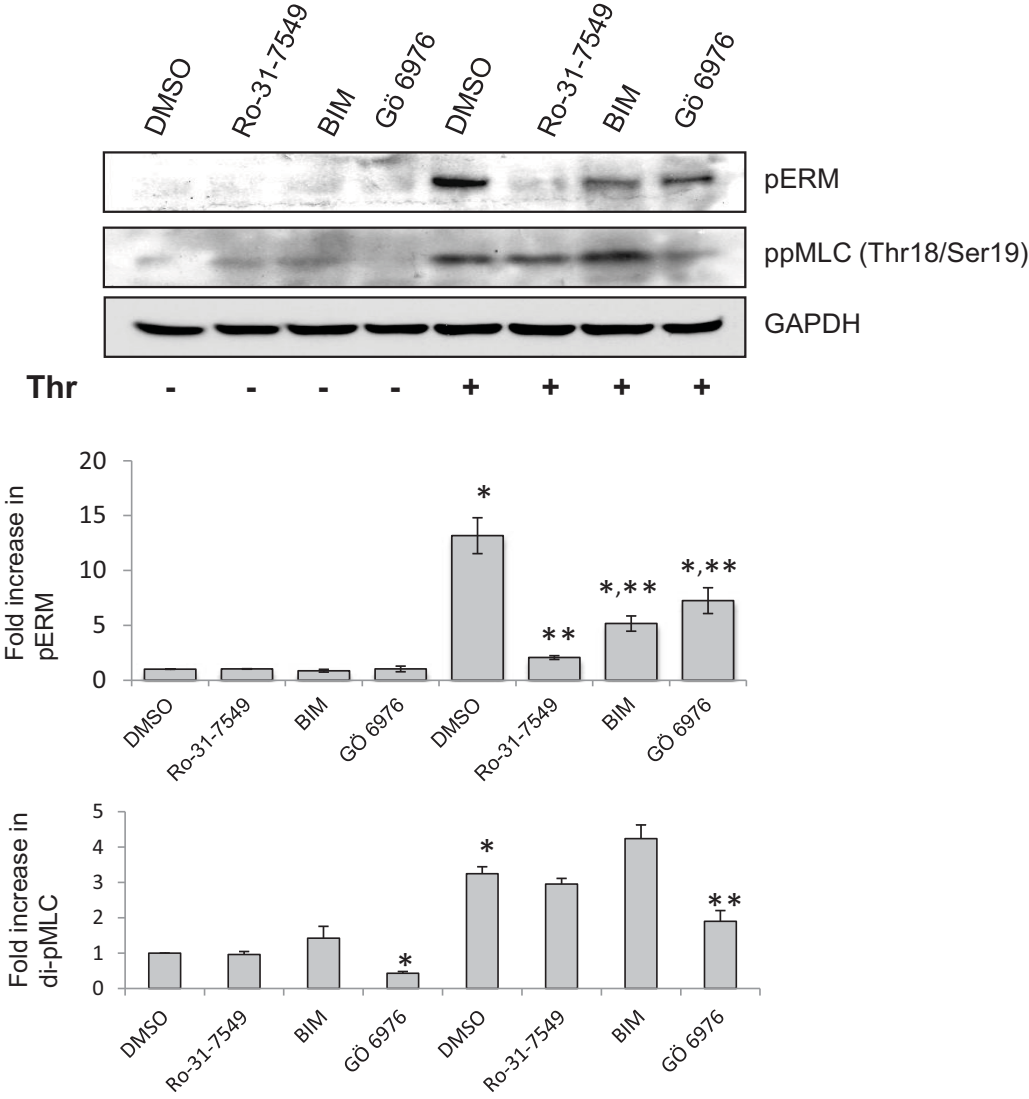


Figure 4A-D

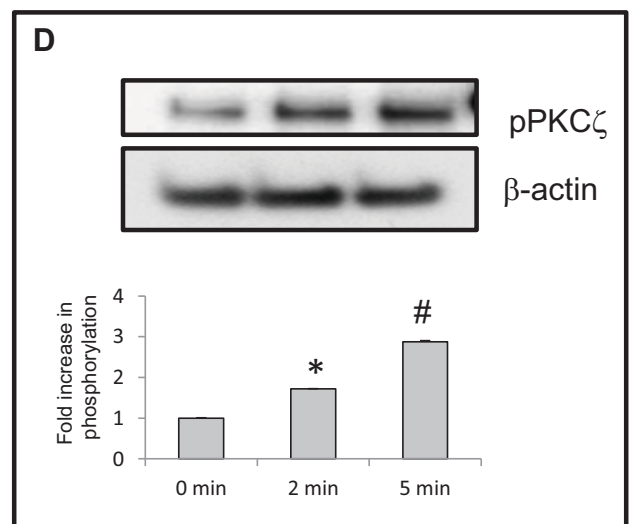
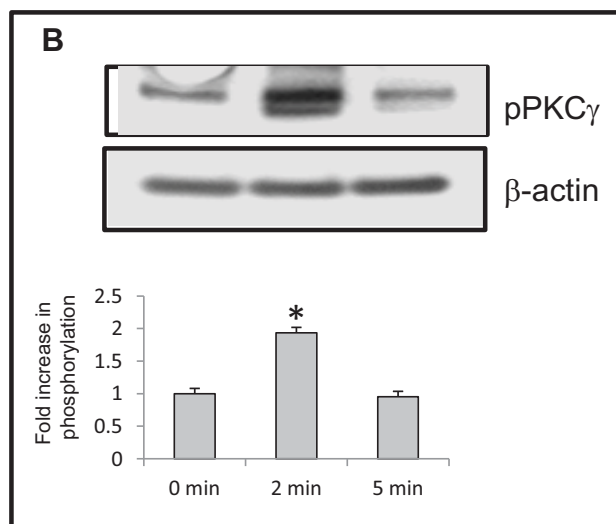
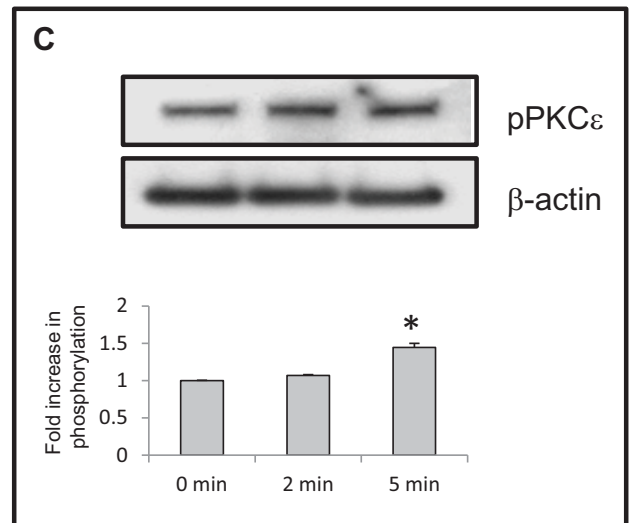
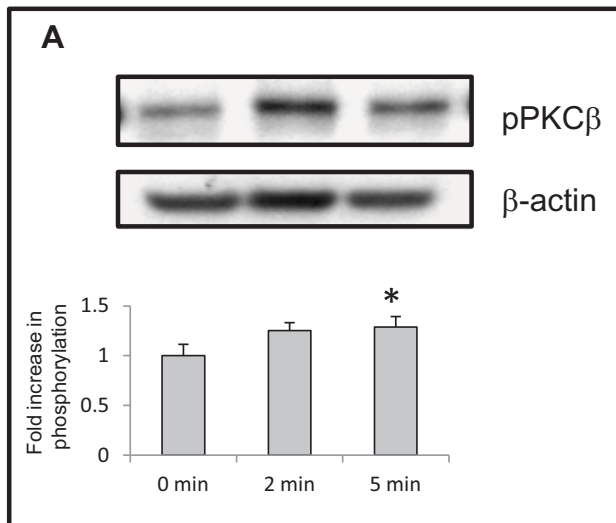


Figure 4E, F

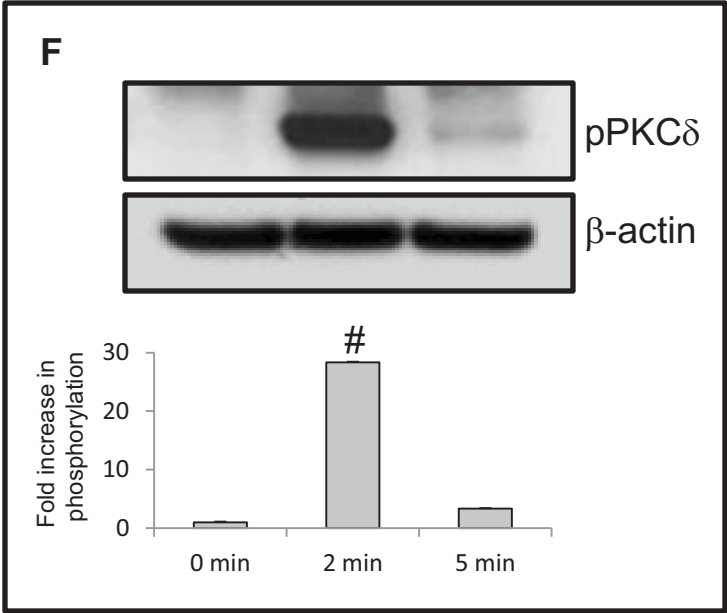
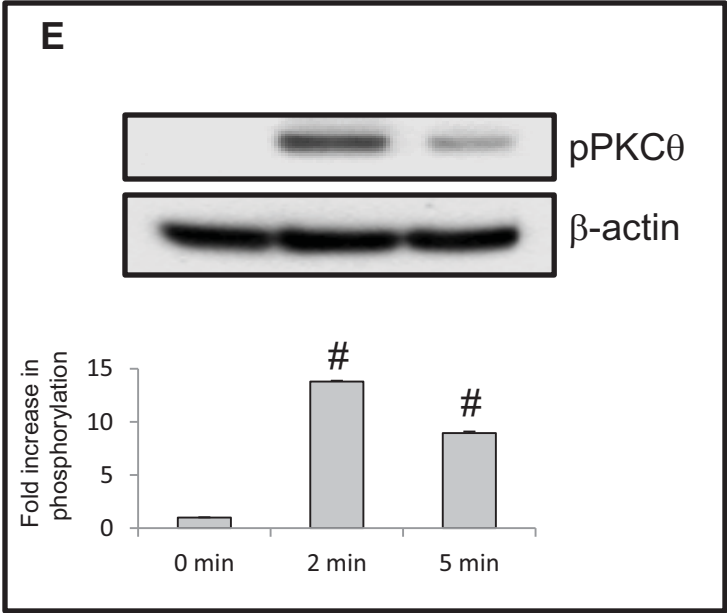


Figure 5

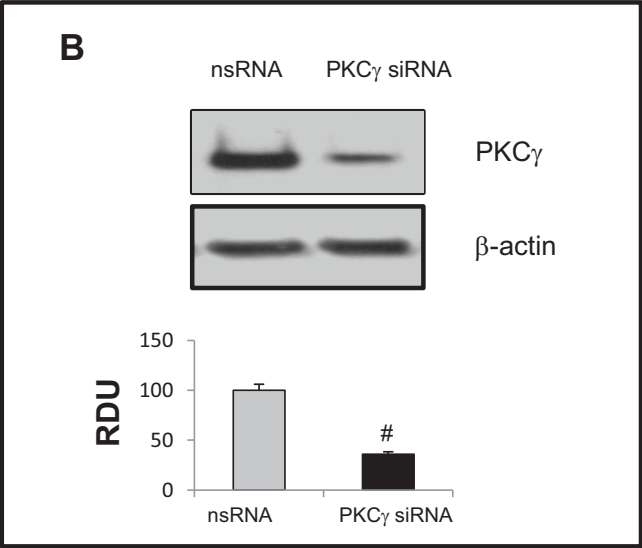
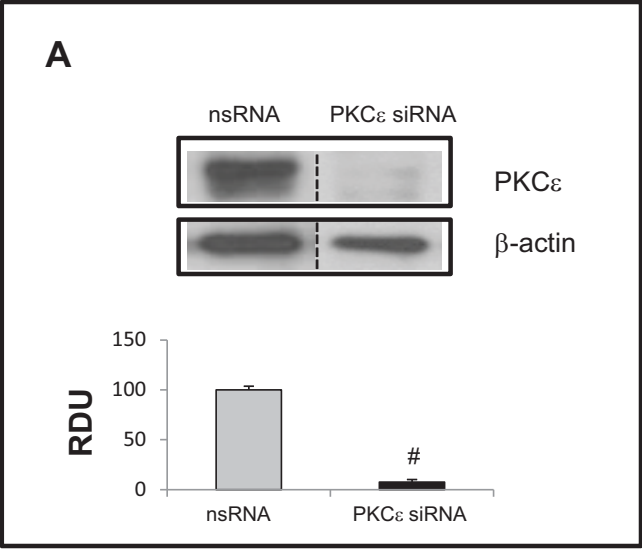
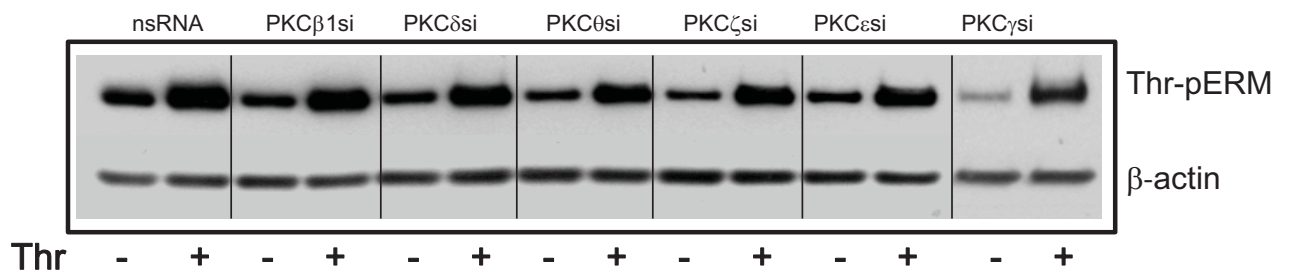


Figure 6A, B

A



B

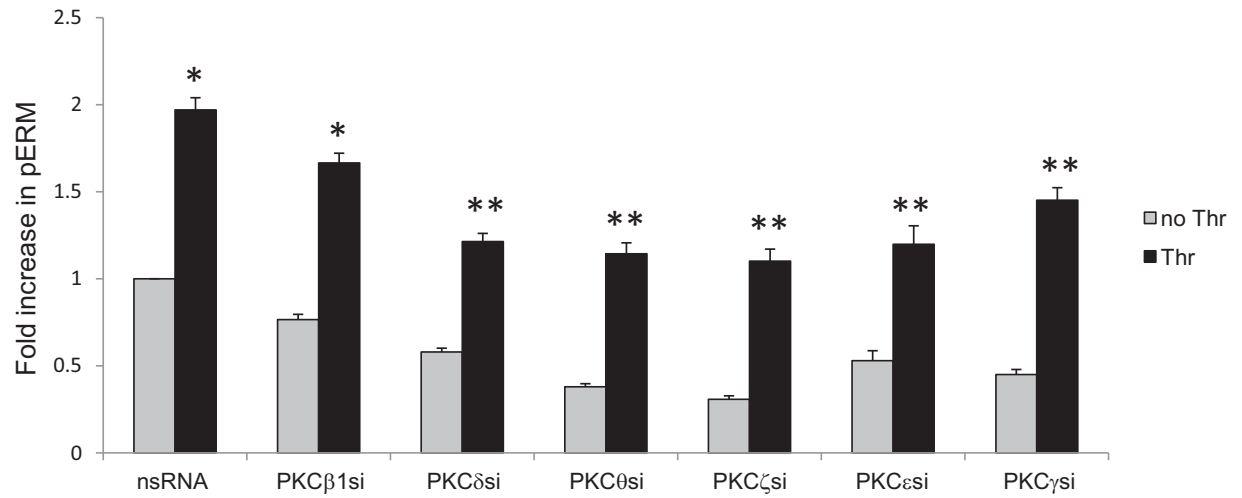
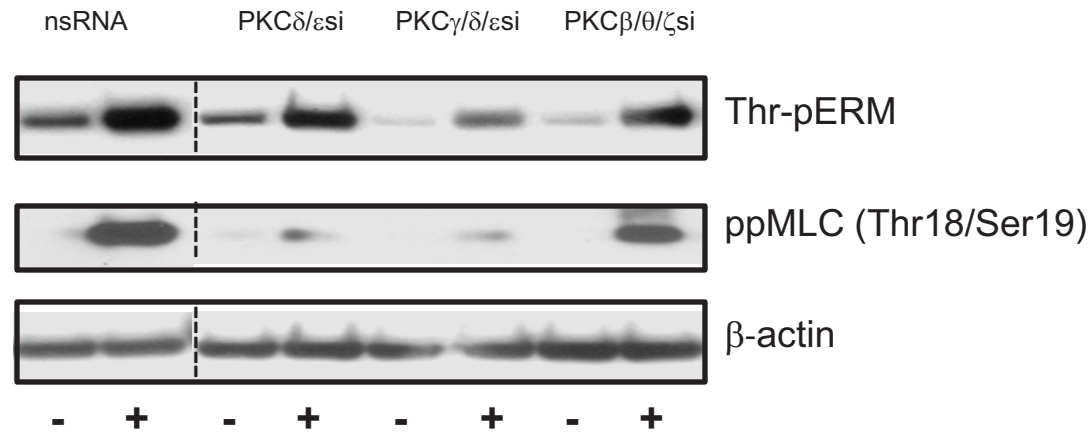
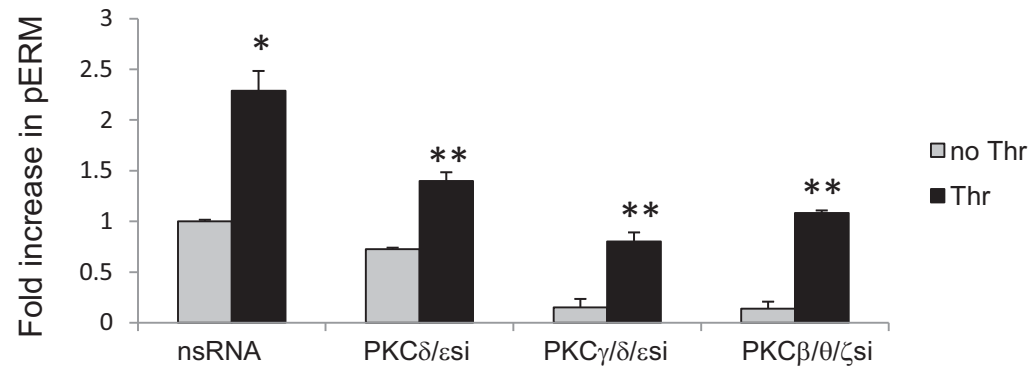


Figure 6C, D, E
C



D



E

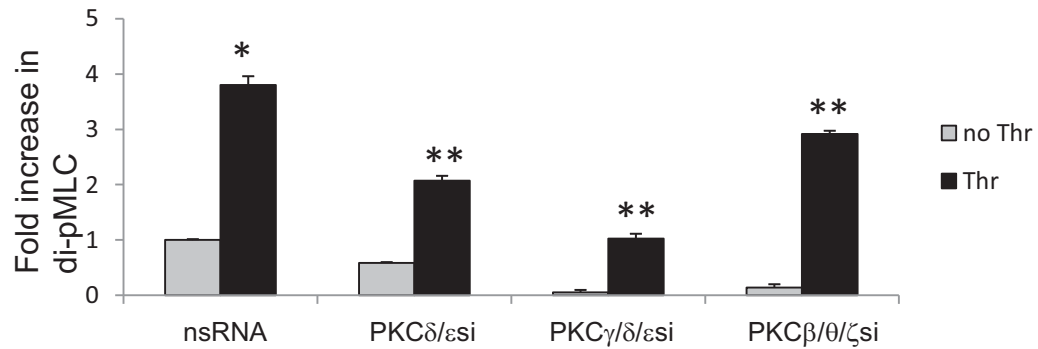


Figure 7A, B

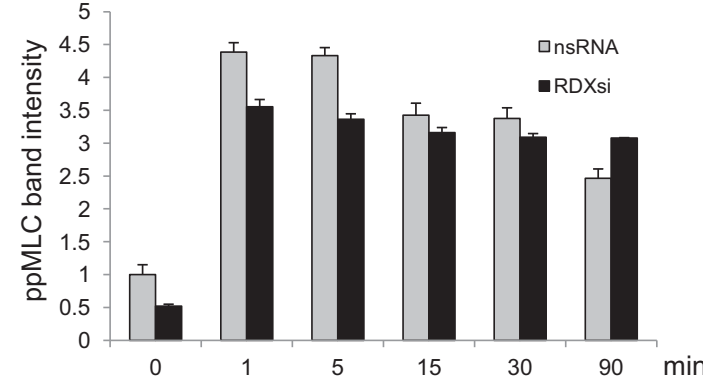
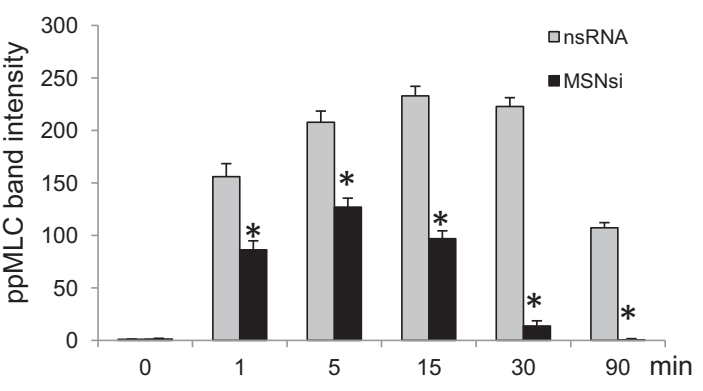
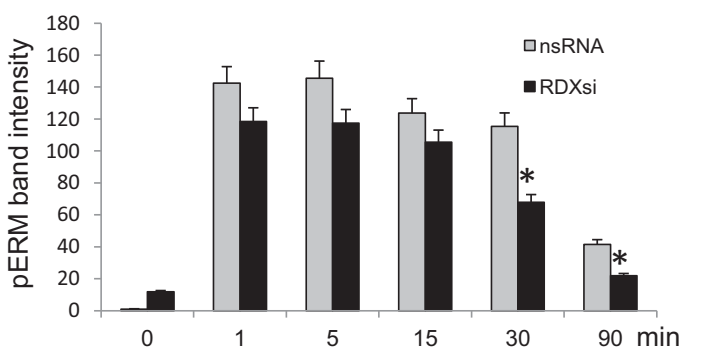
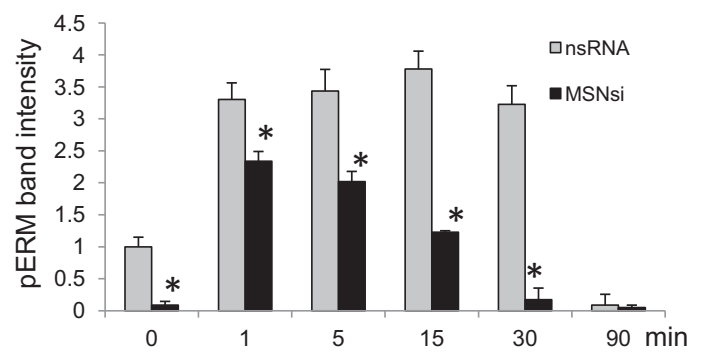
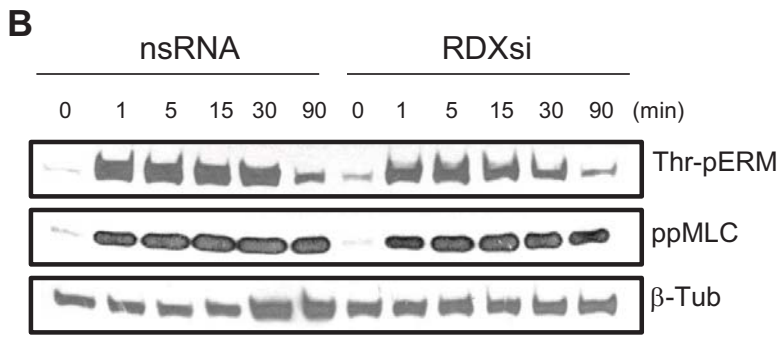
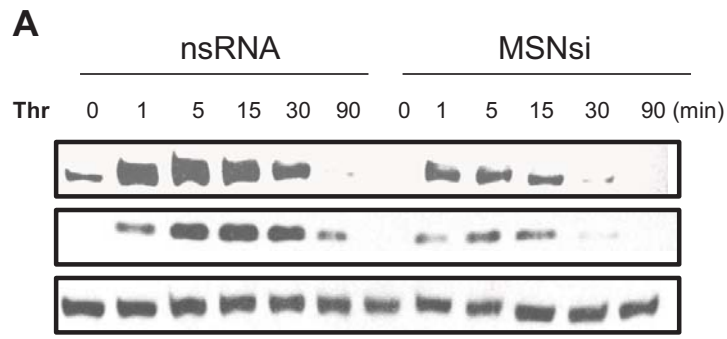


Figure 7C, D

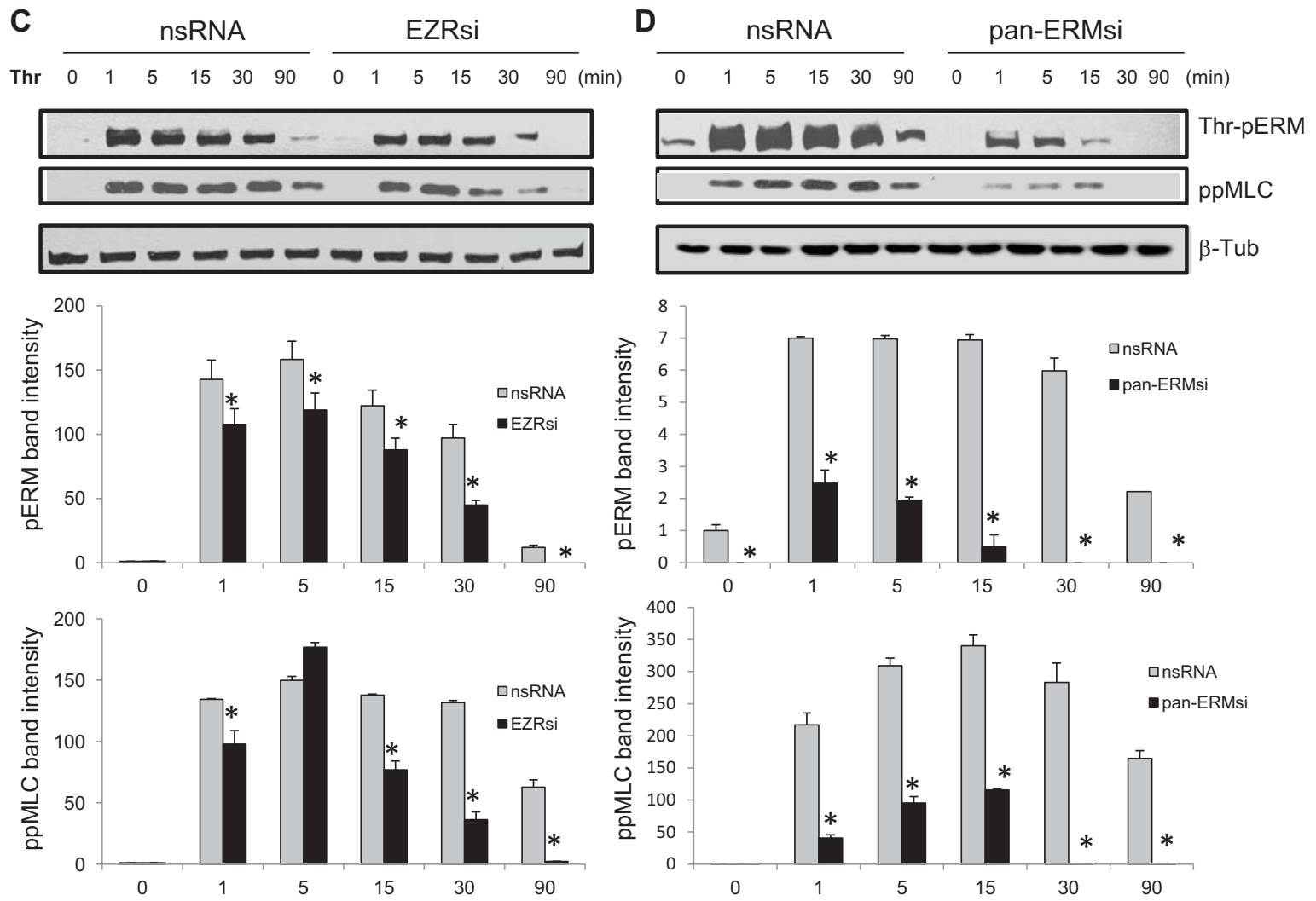


Figure 8A, B

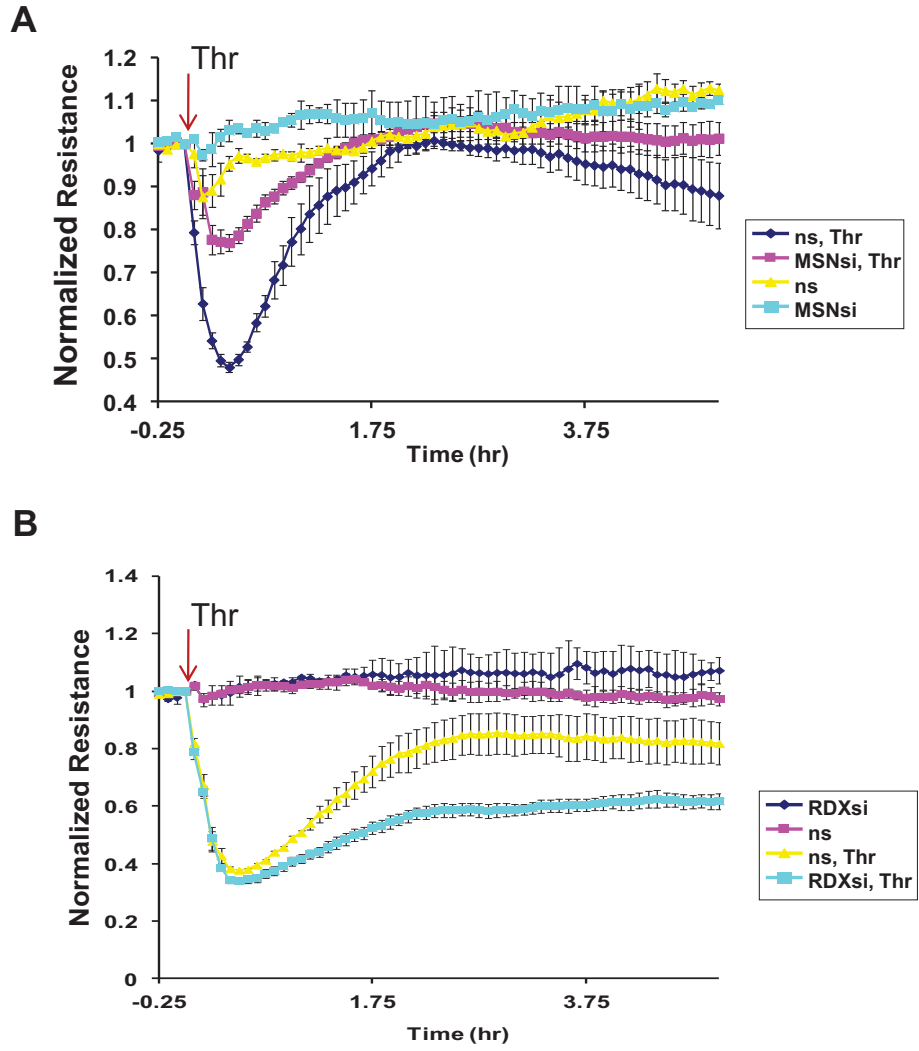
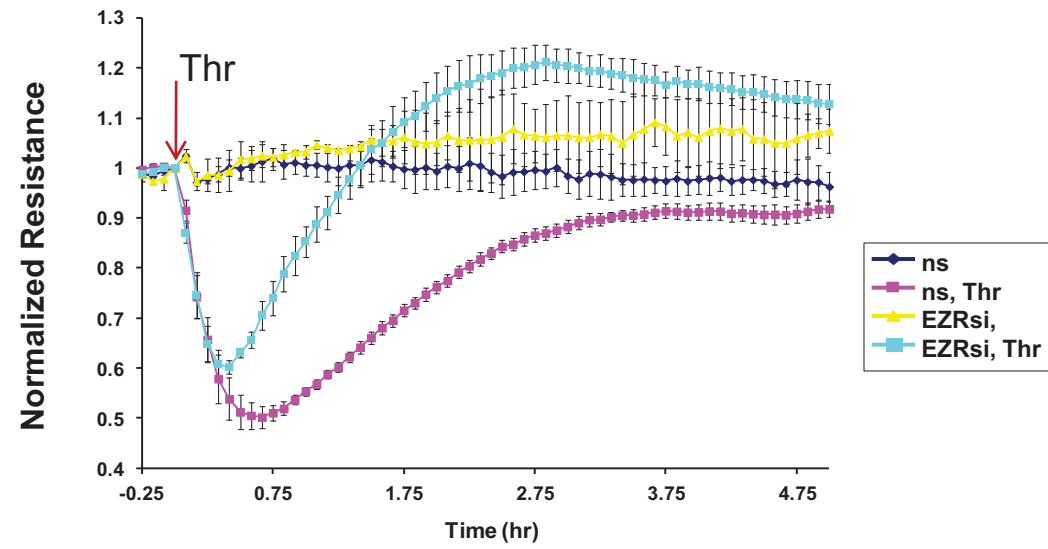


Figure 8C, D

C



D

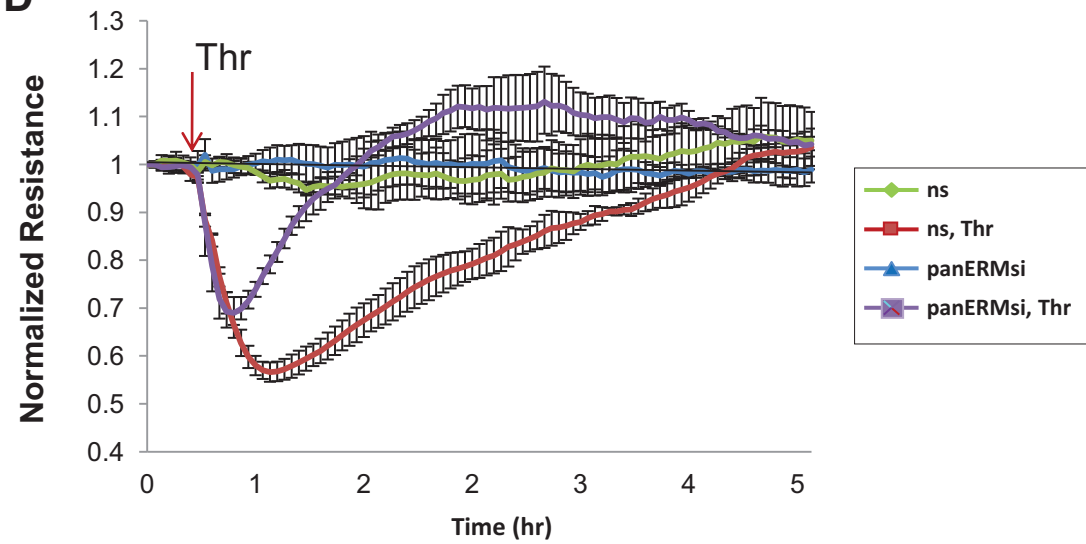


Figure 8E

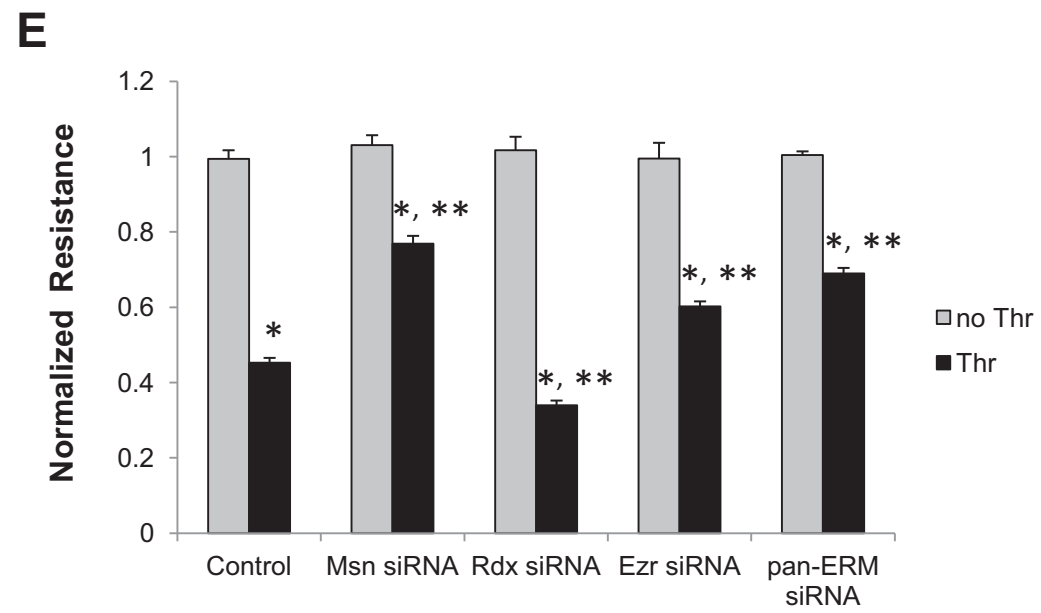


Figure 9

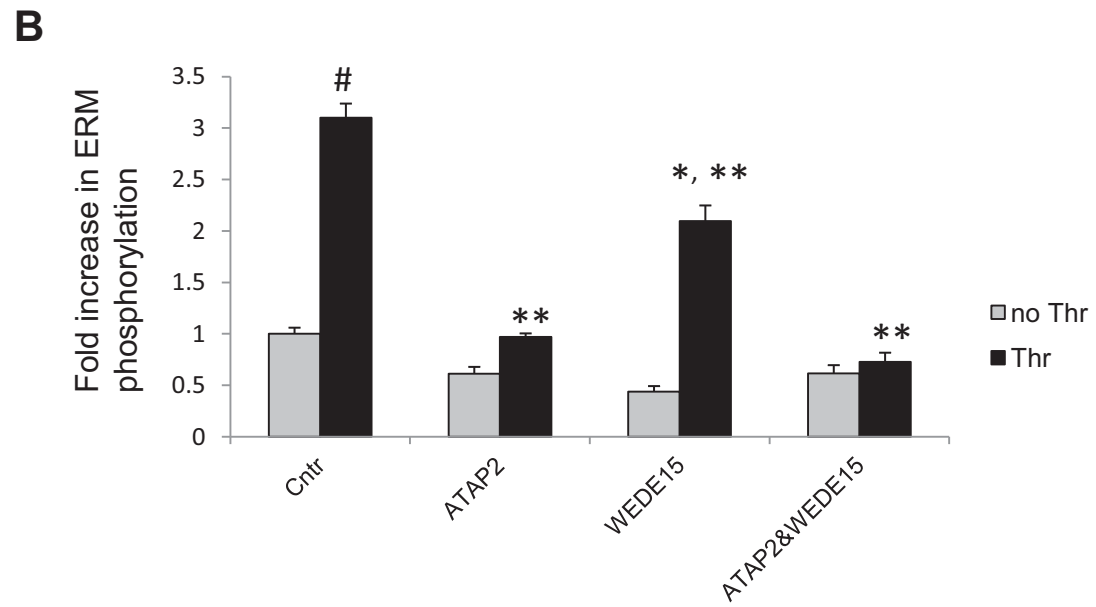
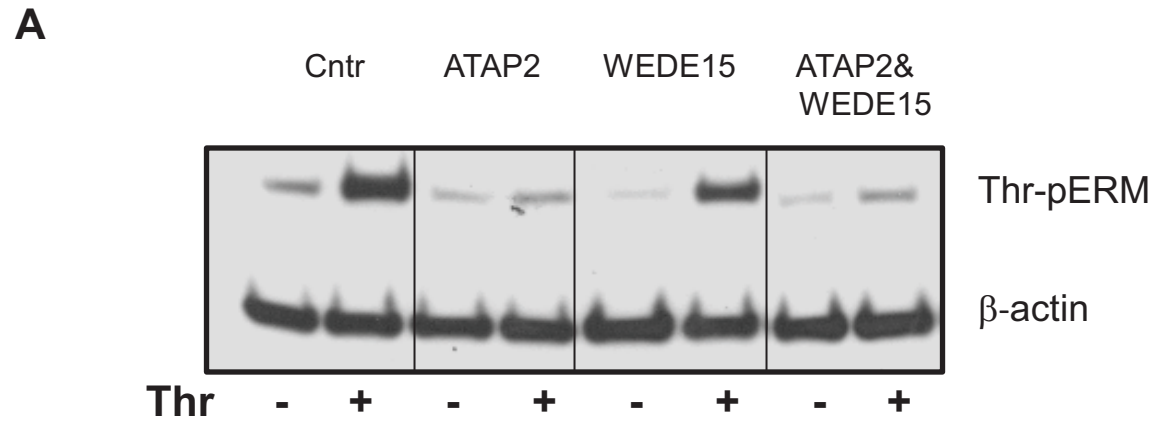
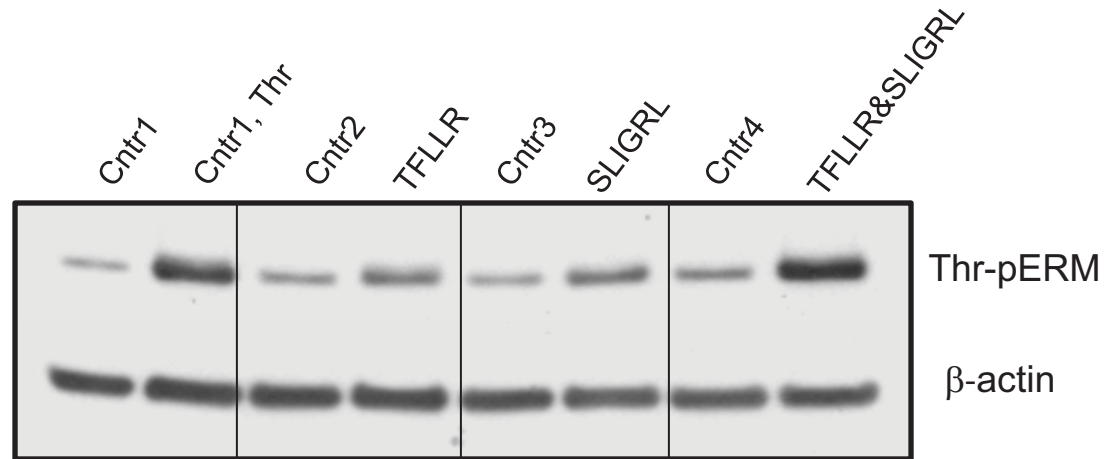


Figure 10

A



B

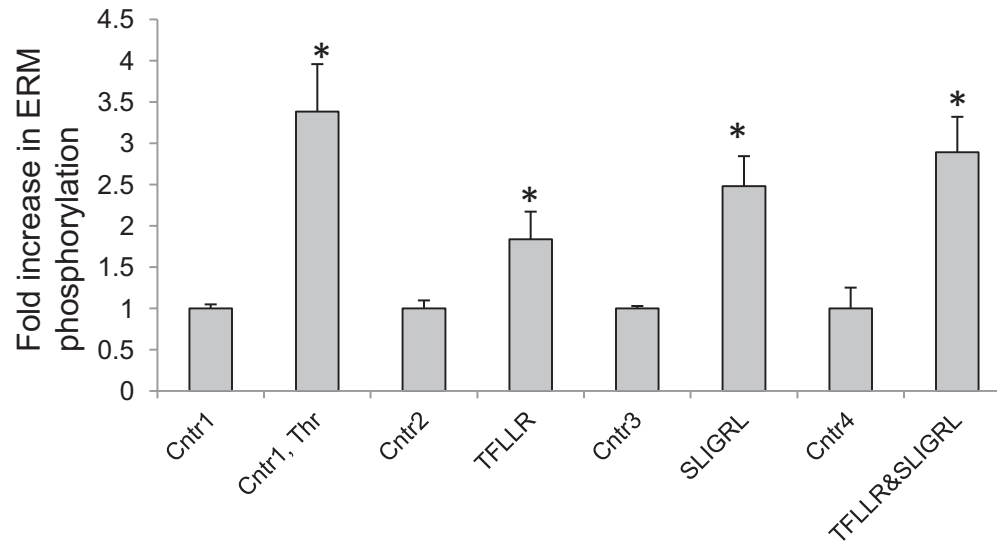


Figure 11

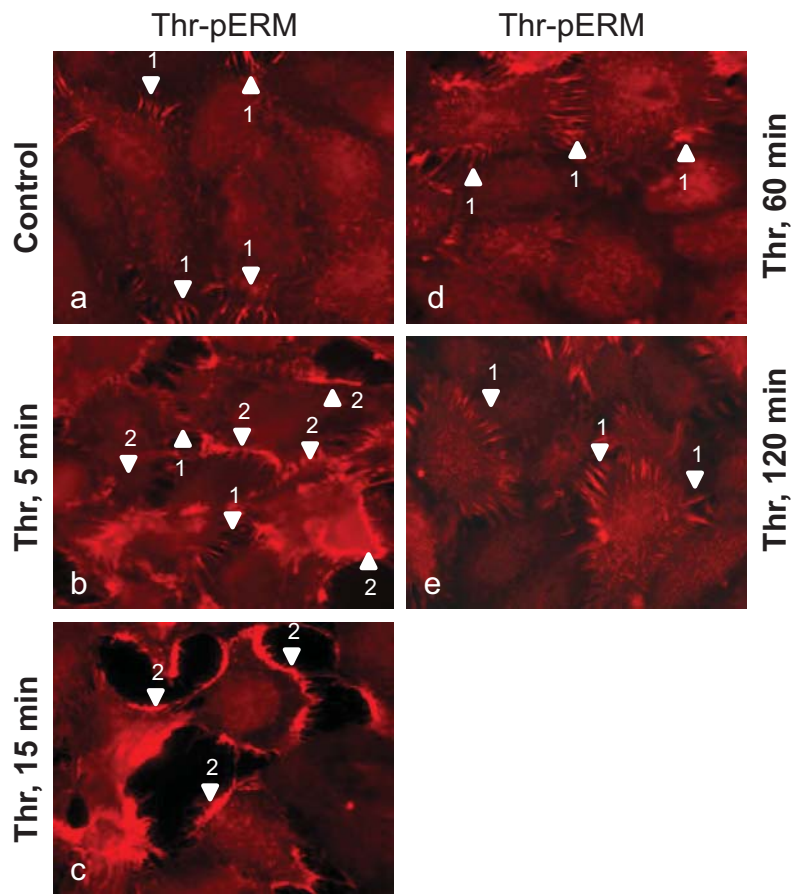


Figure 12

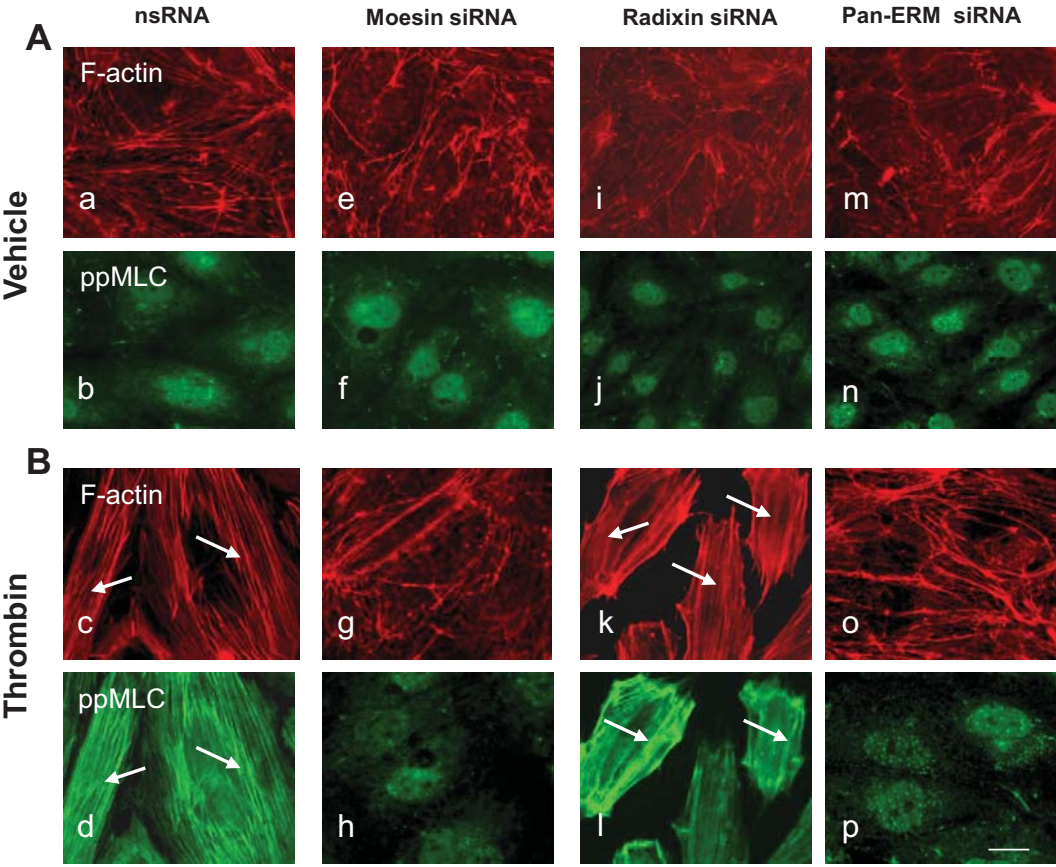


Figure 13

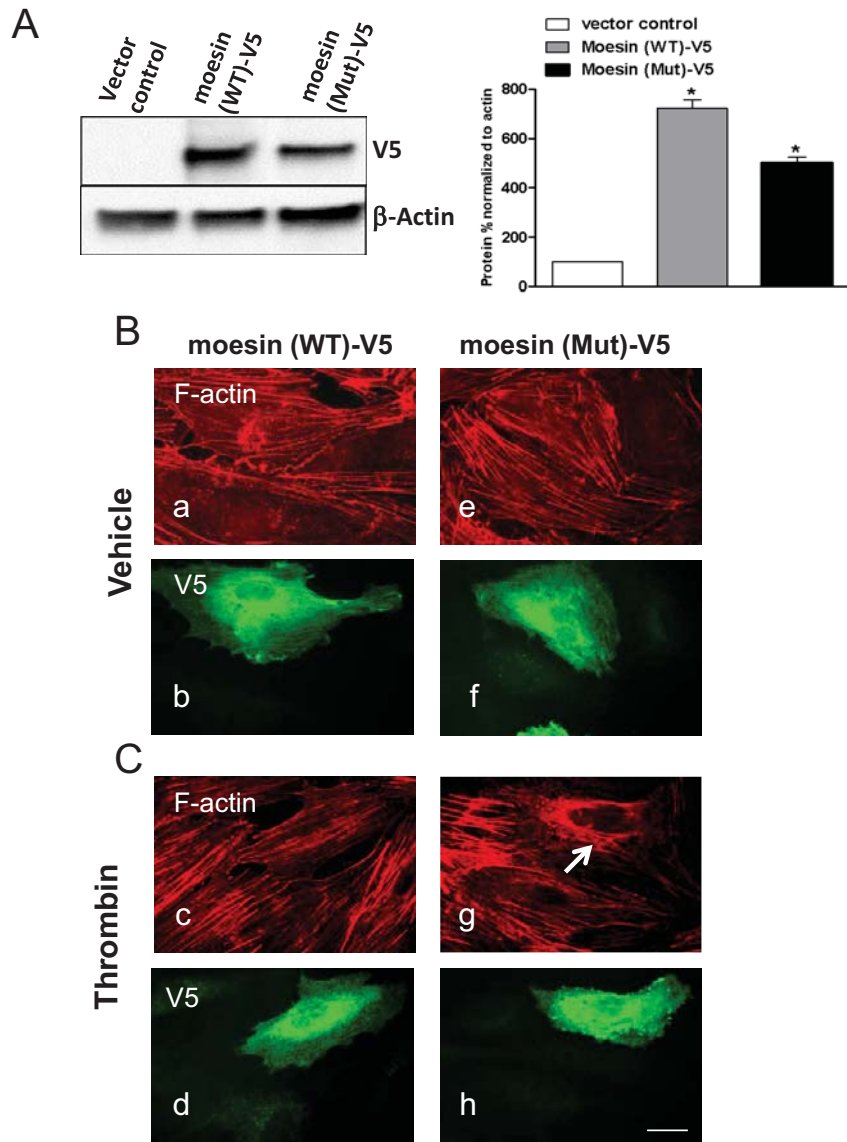


Figure 14

